STUDY OF SELF-DRIVING SYSTEM USING GNSS COORDINATE WITH POSITION CORRECTION ALGORITHM

March 2018

李 熙珍

◇ ◇ ◇ Table of Contents ◇ ◇ ◇

1 Introduction **1**

1.1 Self-driving Technology Vehicle 1

1.1.1 Platooning System 2

1.2 Global Navigation Satellite System (GNSS) 3

1.2.1 Dilution of Precision 5

1.2.2 Ionospheric Passage Error 6

1.3 Research Objectives 7

2 Proposed Self-driving System **9**

2.1 Principle of Self-driving by using GNSS Coordinate 9

2.1.1 Coordination and Tracking Algorithm 9

2.1.2 Obstacle Collision Prevention Algorithm 11

2.1.3 Driving Termination Algorithm 11

2.2 Single Driving Mode 12

2.2.1 Way Point and Destination Setup 12

2.2.2 Way Point and Destination Arrival Judgment Algorithm 12

2.2.3 Throttle Control Algorithm 13

2.3 Platooning Driving Mode 13

2.3.1 Grouping Algorithm 14

2.3.2 Platooning Procedure 14

2.3.3 Throttle Control Algorithm 16

3 Developed Vehicles **17**

3.1 Compact Vehicle Development 17

3.1.1 Parts Configuration 18

3.1.2 Battery System 19

3.1.3 Communication Configuration 19
3.1.4 Microprocessor and Microcomputer 20
3.1.5 Hub-Motor with Hole Sensors 20
3.1.6 Software Differential for Front-wheels 21
3.1.7 Dual Brake System 21
3.1.8 Motor Powered Steering 21
3.1.9 Dual GNSS Module 21
3.1.10 Lidar Sensor 22
3.1.11 Ultrasonic Sensor 22
3.1.12 Dual Digital Compass Sensor 24
3.1.13 LED Light for Human Machine Interface 24
3.1.14 Characteristics of Compact Vehicle 25
3.2 Small-scale Vehicle Development 27

4 Experiment of Self-driving System **29**
4.1 Experiment of Single Mode Self-driving 29
4.1.1 Setup for Test 29
4.1.2 Experiment Result 29
4.2 Experiment of Platooning Mode Self-driving 32
4.2.1 Setup for Tracking and Approaching Test 32
4.2.2 Setup for Position Error Measurement Test 34
4.2.3 Experiment Result 35
4.3 Experiment of Collision Prevent Algorithm 39
4.3.1 Experiment Result 41

5 Proposed Correction Algorithms **43**
5.1 Position Correction by Learning Algorithm 43
5.1.1 Measurement Condition 44
5.1.2 Measurement Result 46
5.1.3 Correction Simulation 47
5.1.4 Learning Result of the HNN 49
5.1.5 Correction Result 52
5.2 Position Correction by Satellite Ephemeris 54
5.2.1 Position Measurement 54

5.2.2 Measurement Result 55
5.2.3 Correction Result 56
5.3 Position Correction by Vehicle Dynamics 57
5.3.1 Correction Algorithm in Driving 57
5.3.2 Correction Algorithm in Stopping 58
5.3.3 Correction Result for Driving 58
5.3.4 Correction Result for Stop 62
5.4 Position Correction by Multiple GNSS 63
5.4.1 Measurement Condition 63
5.4.2 Measurement Result 64
5.4.3 Correction Result 65

6 Conclusion **67**

A Appendix **69**
A.1 CAN Message List and Description 69
A.2 Front Wheel Differential Characteristic 74

References **75**

Publications **83**

Acknowledgments **85**

Chapter 1

Introduction

1.1 Self-driving Technology Vehicle

Recently, the self-driving technology has been rapidly developed in Intelligent Technology (IT) and automotive industries. Figure 1.1 shows a self-driving vehicle which is developed by Google. It is well known that Google shows remarkable performances of the self-driving system which is configured by cameras, radars, the Global Navigation Satellite System (GNSS) device and Google digital map. Generally, the self-driving vehicle operates based on the image processing information by using cameras, radars and GNSS for positioning and obstacle detection [1], [2]. However, it is difficult to use in bad weather situations and when the camera is covered by obstacles. In addition, the use of camera and radar increases the cost of producing the vehicle [3]-[10].

Figure 1.1: Google self-driving vehicle

1.1.1 Platooning System

Platooning driving system is categorized as self-driving [11],[12]. Platooning means a driving series which is of more than two vehicles aligned in one line as a group. Figure 1.2 shows an example of the platooning driving system. Generally, non-leader vehicles follow each of the preceding vehicles [13],[14]. The Leader vehicle is autonomously controlled or driven manually.

The platooning driving system was highly optimized for heavy raw material transportation or a logistics business which needed to drive many vehicles simultaneously. Merits of the platooning system for the end-user are decrease in accidents, increase in aerodynamic performance, increase in fuel efficiency by the shortest distance between vehicles and is available with flexible transportation planning. Merits for the developer are simplification of hardware and software, cost down of the product because almost all of the processing for driving are executed by a leader vehicle [15].

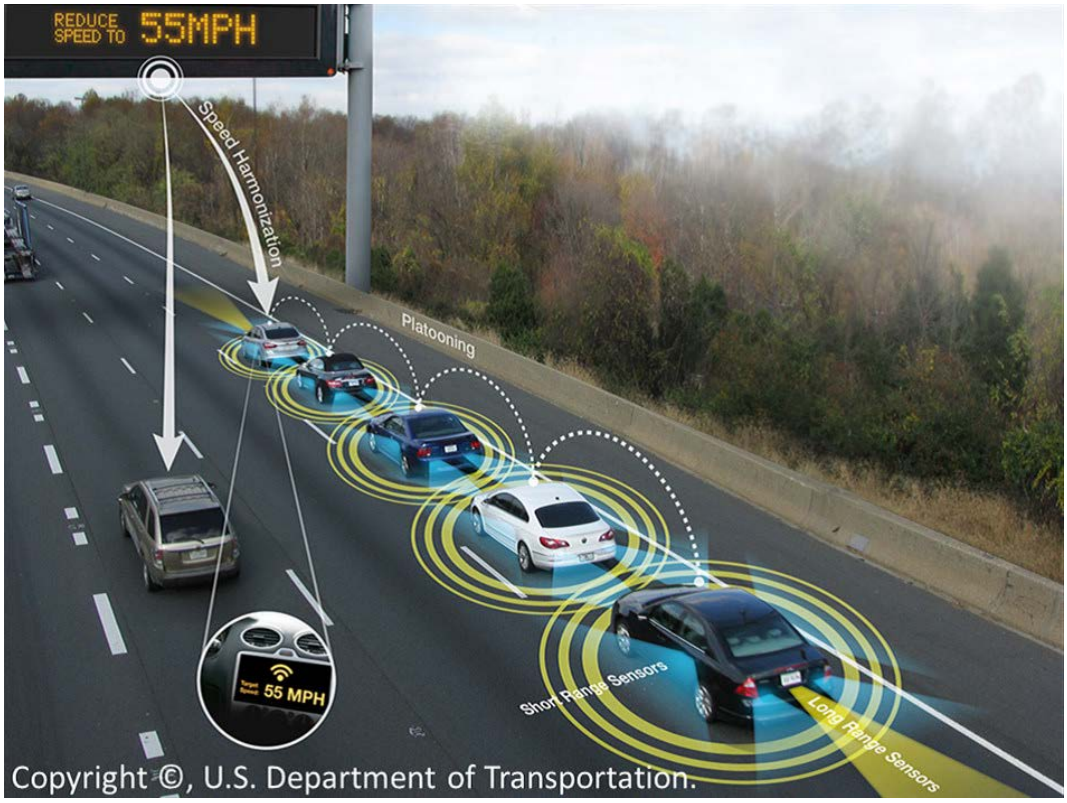

Figure 1.2: Concept of platooning system

1.2 Global Navigation Satellite System (GNSS)

If the GNSS technology, such as Global Positioning System (GPS, USA), GLONASS (RUSSIA) and GALILEO (EU), is used for measuring the correct position of a vehicle, there is no need to measure the vehicle position by using a camera. The GPS is the most useful system at present. The GPS system supplies two services, which are Precise Positioning Service (PPS) and Standard Positioning Service (SPS) [16]. The PPS provides reliable positioning which is enough to implement the self-driving system [17]. However, the PPS can be used only for military or by an authorized user. The SPS is independently operated by only the GPS receiver, while the position is calculated by receiving information from the satellite. The SPS can be used without authorization. However, the positioning reliability of the SPS mode is insufficient for practical use [18]-[24].

Figure 1.3 shows an example of GNSS positioning reliability, indicating the method in two-dimension. The GNSS positioning reliability is quantified to accuracy and precision [25]. Accuracy means how it is close to the absolute coordinate from each measured coordinate. The error of each positioning is quantified to accuracy which is indicated in distance unit. The precision means how concentrated is each measured coordinate, and is indicated in the distribution of each measured coordinates. In this study, the accuracy has been significantly considered for positioning reliability evaluation and position error indication [26]-[32].

Approximately 95% of position errors as accuracy occurred lower than 3.351 m in the SPS mode of GPS [33], [34]. Therefore, self-driving by using the SPS is practically unable. On the other hand, an error correction algorithm, which is possible to increase a positioning accuracy in about several centimeters, is applied under the Differential Global Navigation Satellite System (DGNSS) mode in the SPS mode. In the DGNSS mode, two types could be applied for position correction. One of the types is Real Time Kinematic (RTK) and the other is Satellite-Based Augmentation System (SBAS). In the RTK-type, Radio Technical Commission for Maritime Service (RTCM) correction data is transmitted to a GNSS receiver from a base station [35]. Therefore, in order to use the RTK-type correction, it is necessary to install the base station in advance, and its available range is limited by the base station performances. Thus, the RTK-type

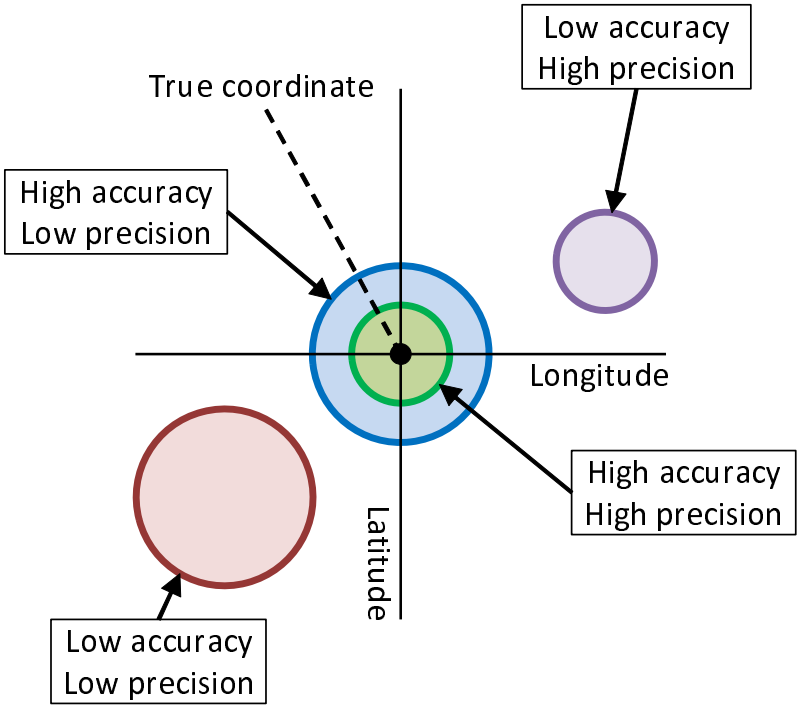

Figure 1.3: The accuracy and the precision in two dimension

is impossible to use under general road environment and is also difficult to use for a self-driving vehicle. In the SBAS-type, correction data is periodically transmitted to a GNSS receiver from the SBAS satellite. Generally, position error is several meters under the SBAS correction. Wide Area Augmentation System (WAAS) of USA or MTSAT Satellite Augmentation System (MSAS) of JAPAN is the most famous for SBAS [36]-[38]. The SBAS is operated with only SBAS compatible receiver, which is not required by the base station. Therefore, although the position accuracy measured by the SPS or the SBAS is not enough for practical use, the SPS or the SBAS mode is available for the self-driving vehicle by using the general road environment [39]-[41].

1.2.1 Dilution of Precision

The signal which is received by GNSS antenna is processed in GNSS module. Processed signal is converted to NMEA0183 sentence in almost all of GNSS modules. Not only current coordinates data but also current receiving status, satellite positions, dilution of precision (DOP) parameter output is available in NMEA0183 protocol [42]. DOP is an indicator for uncertainty of received signal from the GNSS.

Table 1.1 indicates that DOP parameters. PDOP, VDOP and HDOP have direct influence with positioning accuracy of a self-driving vehicle. In this study, HDOP is considered for positioning evaluation and coordinates correction. HDOP is a value from PDOP without the altitude component. Equation (1.1)- Equation (1.5) describe relations between DOPs. A lower HDOP means a higher positioning reliability,

Table 1.1: DOP parameters and descriptions

Parameter	Description
GDOP	Geometric DOP
PDOP	Position DOP
TDOP	Time DOP
VDOP	Vertical DOP
HDOP	Horizontal DOP
NDOP	Northing DOP
EDOP	Easting DOP

$$GDOP = \sqrt{\sigma_{Lon}^2 + \sigma_{Lat}^2 + \sigma_{Alt}^2 + \sigma_{Time}^2}/\sigma \tag{1.1}$$

$$TDOP = \sqrt{\sigma_{Time}^2}/\sigma \tag{1.2}$$

$$PDOP = \sqrt{\sigma_{Lon}^2 + \sigma_{Lat}^2 + \sigma_{Alt}^2}/\sigma \tag{1.3}$$

$$VDOP = \sqrt{\sigma_{Alt}^2}/\sigma \tag{1.4}$$

$$HDOP = \sqrt{\sigma_{Lon}^2 + \sigma_{Lat}^2}/\sigma \tag{1.5}$$

where σ_{Lon}^2 , σ_{Lat}^2 , σ_{Alt}^2 are the variances of the longitude, latitude and altitude components. σ_{Time}^2 is the variance of the module clock offset estimate. σ is the overall standard deviation in range [43].

1.2.2 Ionospheric Passage Error

It is well known that the position errors occur in a satellite orbit error, an atomic clock error, an ionosphere passage, a troposphere passage, a multi path, due to the arrangement of satellite geometric error. The largest component of reason in the position error is the time delay by the ionospheric passage [44]. Figure 1.4 shows the correlation between refraction and propagation delay on the ionospheric passage.

Radio wave refraction occurs when the radio wave passes through the ionosphere and the path of radio wave becomes longer. The ionospheric delay depends on the relative position between satellite and receiver. If the satellite on the high elevation is close to 90 degrees in the sky from the receiver, the radio wave is passed perpendicularly to the surface of the ionosphere. In this situation, the ionospheric delay is minimized as close as to zero. Conversely, in a situation of low elevation close to 0 degree, the ionospheric delay is maximized. However, if two SPS mode GNSS receivers are located close to each other, the trends of each position error are similar. This is the reason why there is a greater possibility that two SPS mode GNSS receivers receive signal from the same satellites located near each other in approximately 10 km [45]. That is, it causes a similar time delay, since signals received by two SPS mode GNSS receivers are passing through a similar path of ionosphere passage. Therefore, position errors have similar trends between two receivers [46].

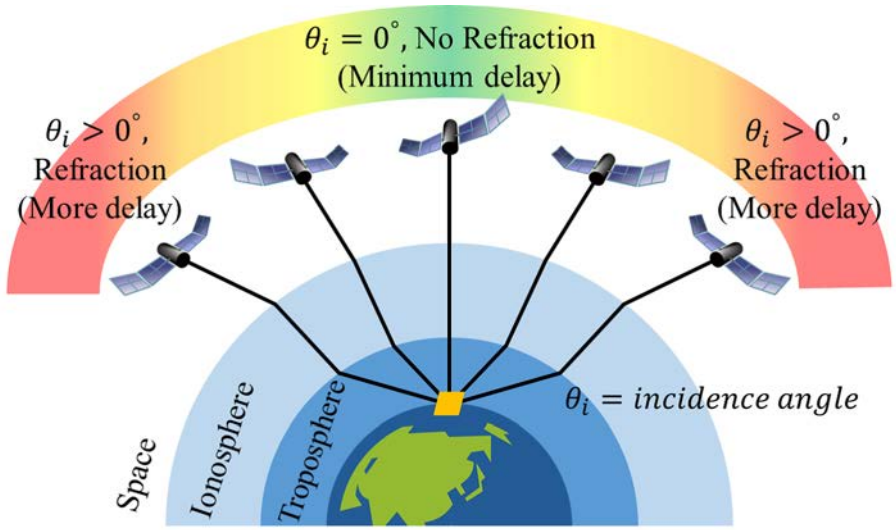

Figure 1.4: Propagation delay by refraction on the ionospheric passage

1.3 Research Objectives

In this study, two types of simple and low-cost self-driving systems are proposed. The systems are constructed without cameras-based image processing. Two types of vehicle are automatically controlled with tracking to the destination coordinates or preceding vehicle. One vehicle is a compact vehicle which is available to boarding maximum two passengers. The other is a small-scale vehicle which is controlled by a radio controller, originally.

In order to improve positioning stability and reliability, several position correction algorithms are proposed to the system.

In addition, to ensure safety of the self-driving, obstacle detection and collision prevent stop function is implemented with several sensors.

System algorithm, implementation and evaluation method are described in detail. Several experimental and simulation results by using developed vehicles demonstrate the validity of the proposed system and correction method.

Chapter 2

Proposed Self-driving System

2.1 Principle of Self-driving by using GNSS Coordinate

In the self-driving system of this study, current coordinate and targeted coordinate are continuously compared to determine throttle and steering of the vehicle. There are two types of self-driving modes. One is single self-driving mode and the other one is platooning self-driving mode.

In the single self-driving mode, the targeted coordinate is a fixed coordinate on Earth. However, in the platooning self-driving mode, the target coordinate is a dynamic coordinate which is a current coordinate of the preceding vehicle.

In the case of the vehicle is in danger from high probability of collision with something obstacle, vehicle reduces velocity or stops itself. The vehicle resumes self-driving after escapes from dangerous situation. If self-driving is not in continual situation, the vehicle forced terminates self-driving itself [47].

2.1.1 Coordination and Tracking Algorithm

Figure 2.1 shows a relation of current coordinate and target coordinate [48]. The triangular function is used for calculating of distance to remain, target azimuth, target angle for destination or preceding vehicle. The relative distance is calculated by equation (2.1).

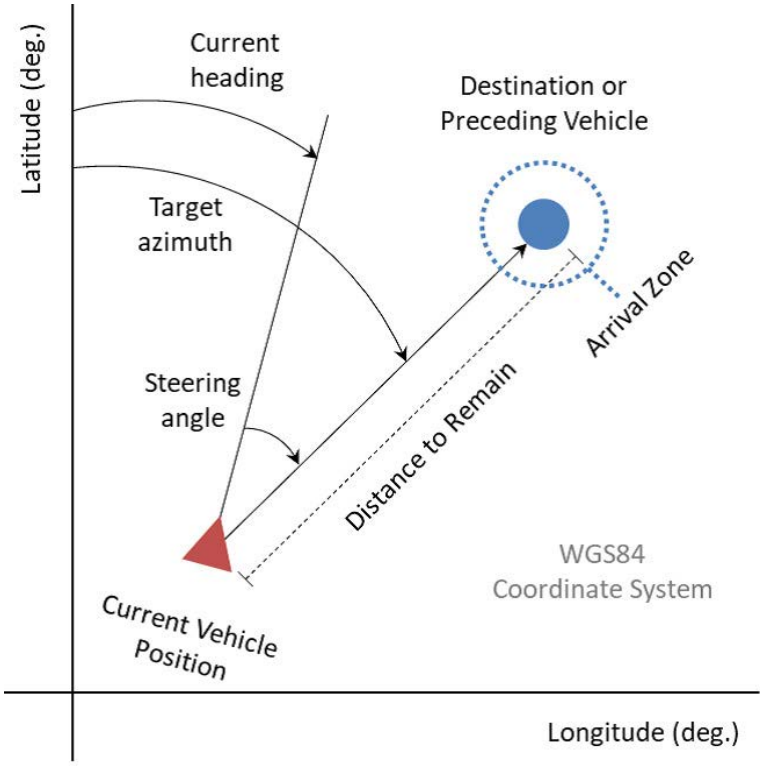

Figure 2.1: Coordination and target setup

$$s = \sqrt{\left\{\left(\frac{2\pi r}{360}x_{p-f}\right)\cdot\cos\left(\frac{\pi}{180}y_f\right)\right\}^2 + \left(\frac{2\pi r}{360}y_{p-f}\right)^2} \tag{2.1}$$

where s is the relative distance which can be calculated from the difference in longitude x_{p-f} and latitude y_{p-f}. y_f is the latitude of the following vehicle. r is the radius of the earth as approximately 6378.137 km. α denotes the relative angle which can be calculated by equation (2.2).

$$\alpha = \left(\frac{180}{\pi}\right)\cdot\tan^{-1}\left\{\frac{y_{p-f}}{x_{p-f}\cdot\cos\left(\frac{\pi}{180}y_f\right)}\right\} \tag{2.2}$$

2.1.2 Obstacle Collision Prevention Algorithm

Figure 2.2 shows obstacle detection zone and stop zone when the vehicle speed is approximately 5 km/h. The stop zone is extended when the vehicle velocity becomes faster. When the obstacle position is in the stop zone, vehicle reduces velocity and stops itself. The stop zone is determined by vehicle body width, braking performance and safety [49]-[55].

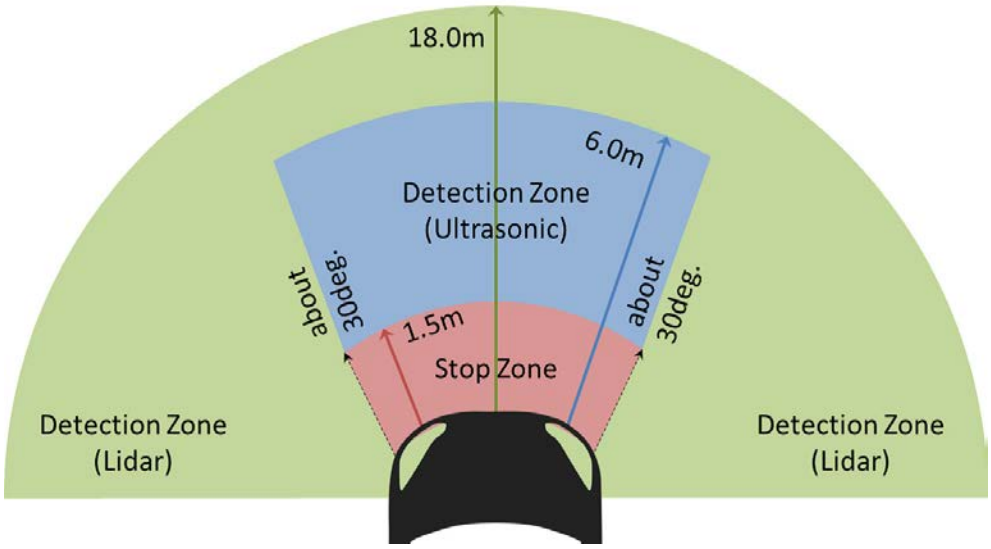

Figure 2.2: Obstacle detection and stop zone at 5 km/h

2.1.3 Driving Termination Algorithm

The group driving could be terminated by the GNSS receiver fault, relative distance, relative heading angle. If the GNSS operation mode in DGNSS SBAS and positioning data is available, the GNSS positioning data can be used to calculate for driving. On the other hand, in the case of the GNSS operation mode in 2D or invalid, the positioning data is not available. The system converts current latitude to 99 degree and current longitude to 199 degree for the processing coordinate to be invalid. Therefore, the driving is terminated by an invalid coordinate. If the relative distance is over 110 m, the system terminates driving. The system limits maximum velocity to 200 km/h. In this case, according to typical traffic rules, the safety relative distance between preceding vehicle and following vehicle is approximately 110 m [56], [57]. Thus, considering the

safety distance and many types of vehicle, the maximum relative distance is limited to approximately 200 m. If the relative heading angle is over 90 degrees, system terminates the driving. The reason why, the vehicle could be driven in reverse or the reverse direction with high probability.

2.2 Single Driving Mode

In the single self-driving mode, a vehicle drives with tracking to a coordinate of way point or final destination, independently. From the starting point to final destination point, temporary destination coordinate is changed to each way points for tracking each section in route.

2.2.1 Way Point and Destination Setup

Route profile includes every coordinate of way point and destination point with each point number. The coordinates have latitude and longitude components which are based on the WGS84 global coordinate system. Short distance between way points is better for self-driving accuracy. However it must be longer than the minimum turning radius. There are two types of route. One is a ring type route. The other is a one way route. The vehicle always tracks lower number way point to high number way point. When the vehicle arrived at the last number point as the final destination, the route type is checked by the system. If the route-type is a ring, way number is reset to initial number. The vehicle tracks initial way point and drives continuously. If the route-type is one-way, the vehicle stops at the final destination point and terminates self-driving itself.

2.2.2 Way Point and Destination Arrival Judgment Algorithm

When the vehicle arrives at the way point or destination point, the system changes temporary destination coordinate to the next temporary destination coordinate. In this situation, in order to judge the arrival on way point or destination point, the system compares current temporary coordinate with current coordinate of the vehicle. When the distance between coordinates is shorter than minimum turning radius, the system judges that the vehicle arrives on current temporary destination.

2.2.3 Throttle Control Algorithm

In the single self-driving mode, target vehicle velocity is determined by a passenger. The vehicle controls vehicle velocity to target velocity by RPM feedback of the left and right wheel. Maximum steering angle is limited by current velocity of vehicle because to prevent a dangerous sharp turn. Figure 2.3 indicates the steering angle limit.

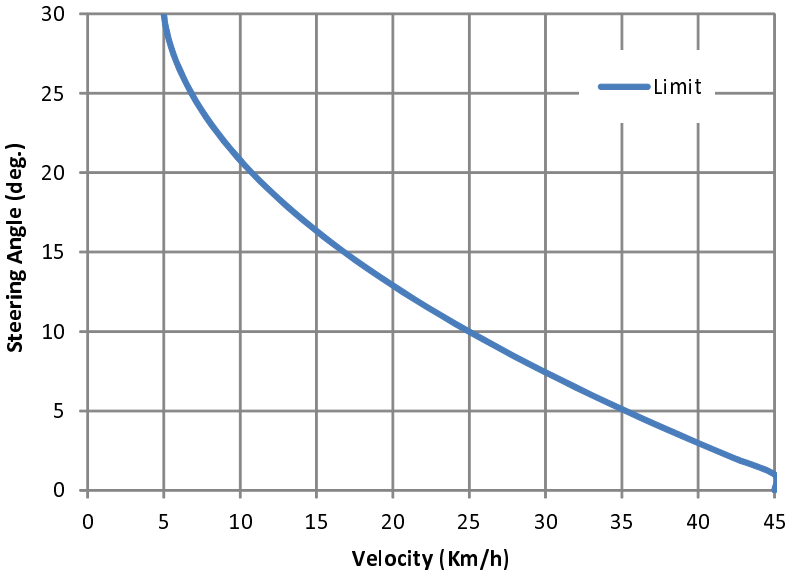

Figure 2.3: Steering angle limitation by velocity

2.3 Platooning Driving Mode

Figure 2.4 shows the concept of the proposed platooning self-driving. The system is configured by the preceding and following vehicles. As mentioned above, the SPS or SBAS of GNSS position errors of vehicles are similar when vehicles are very closely located. Therefore, it is possible to ensure a reliable accuracy by using the relative position of vehicles. The preceding vehicle transmits own position, heading angle and speed to the first following vehicle. The first following vehicle drives by tracking the coordinate of the preceding vehicle, and the second following vehicle drives with tracking a coordinate of the first following vehicle. The preceding vehicle is manually controlled by the driver. Each vehicle updates own position, periodically.

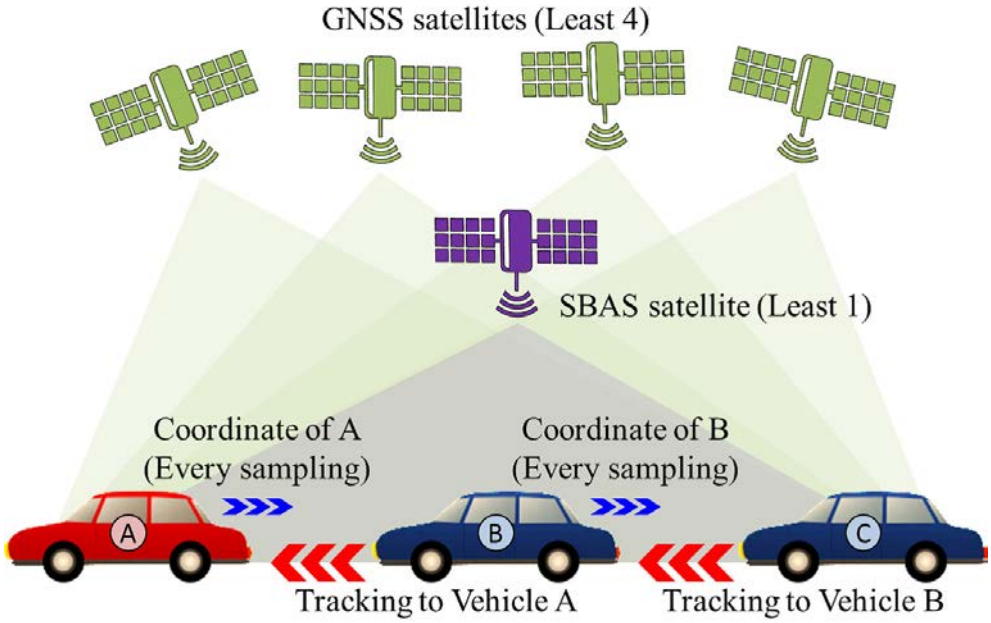

Figure 2.4: Concept of developed platooning mode self-driving

2.3.1 Grouping Algorithm

The preceding vehicle makes a group driving profile, and broadcasts profile to all of the following vehicles in the group. The profile is composed of a number of vehicles, serial number of vehicle, sequence, limit velocity, minimum safety distance. The following vehicle checks the profile, and makes a decision to accept or reject in joining the group. When the following vehicle leaves the group, the following vehicle transmits a request message to preceding vehicle. The preceding vehicle makes the group profile again without requesting the following vehicle. When the preceding vehicle leaves the group, the first following vehicle will be a new preceding vehicle.

2.3.2 Platooning Procedure

Figure 2.5 shows a process flow of the proposed system for the preceding vehicle. Time and position of the preceding vehicle is received from the GNSS receiver module in the DGNSS mode, which is the SBAS type. The GNSS receiver output several messages of the National Marine Electronics Association (NMEA) 0183 format. Time, position and fix related data of the receiver, the GNGGA message is used for calculation

in the algorithm. On the other hand, current heading angle is measured by the digital compass module. The heading angle is corrected -7.3 degrees due to influence of local magnetic field in the Tokushima prefecture, JAPAN [58]. Coordinate from the GNSS receiver is converted to the degree format. Vehicle velocity and throttle is checked by the system. All status of the preceding vehicle is transmitted to the following vehicle and monitoring server. The system updates position and periodically control command every GNSS sampling time.

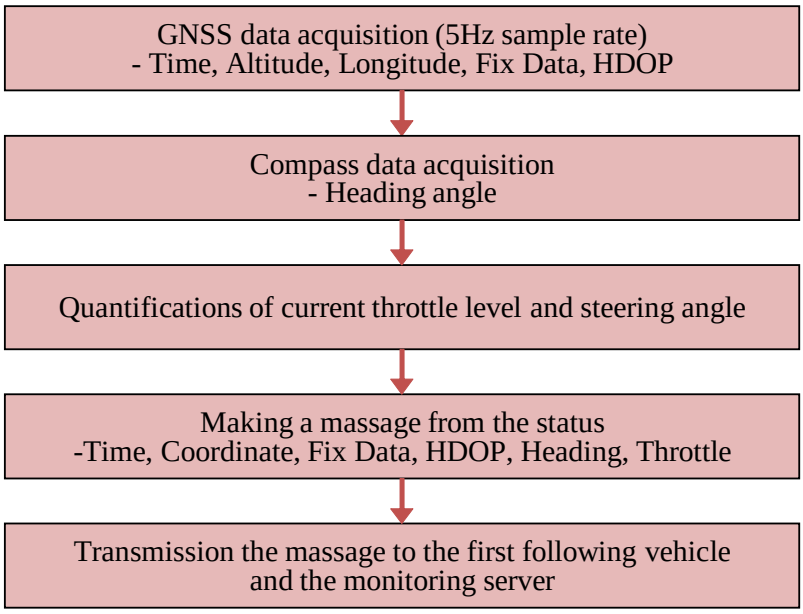

Figure 2.5: Process flow of the preceding vehicle

Figure 2.6 shows a process flow of the proposed system for the following vehicle. The current time and position of the following vehicle are received from the GNSS receiver module in the DGNSS mode, which is the SBAS type. Simultaneously, The status massage of the preceding vehicle is received via a wireless data networking device. In the same way as the preceding vehicle, current heading angle is calculated by the digital compass module. Relative distance and angle are calculated on the bases of each position of two vehicles.

If the relative distance is longer than the target distance, system increases velocity by throttle control. Otherwise, system reduces velocity until reaching at the target distance. The steering angle is controlled by comparing the target angle with current angle. Update period for the position is set to 0.2 second. Calculation period for direction angle and vehicle velocity is set to approximately 0.01 second.

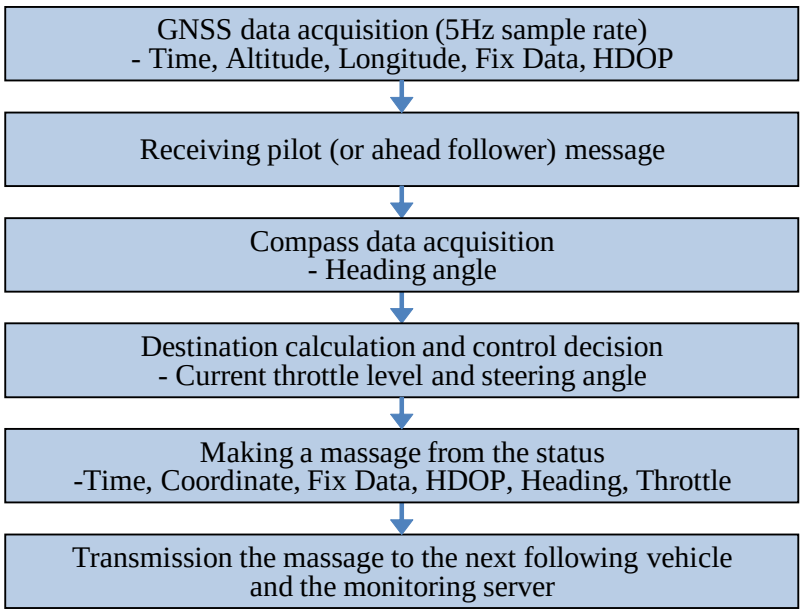

Figure 2.6: Process flow of the following vehicle

2.3.3 Throttle Control Algorithm

In the platooning mode, following vehicle velocity is synchronized with preceding vehicle. The target velocity of preceding vehicle is determined by the passenger. The following vehicle calculates distance for the preceding vehicle every sampling time. If the distance is longer than defined distance, the vehicle increases throttle to reach the defined distance. If the distance is shorter, vehicle reduces throttle.

Chapter 3

Developed Vehicles

3.1 Compact Vehicle Development

Figure 3.1 shows a developed compact vehicle. The vehicle is electric-powered by battery. A maximum of two passengers are available on board. This vehicle is used for single mode self-driving test and evaluation of the multiple GNSS correction method.

Figure 3.1: Developed compact vehicle

3.1.1 Parts Configuration

Figure 3.2 shows a configuration of the electrical and mechanical parts. Batteries are loaded at the chassis bottom. Hub-motors are installed for front wheels. Hole-sensors are included in the Hub-motor. Power steering motor is installed for direction control. For braking, regeneration brake and disc brake are available in the vehicle. Disc brake is actuated by motor. Dual GNSS modules are installed for positioning. In order to detect obstacle, Lidar and ultrasonic sensor are installed. Dual digital compass sensors are installed for vehicle heading angle check. Three axis accelerometer and three axis gyro sensors are installed for vehicle dynamics monitoring and control. Eight LED light modules are installed on front and rear bumper for Human Machine Interface (HMI) [59].

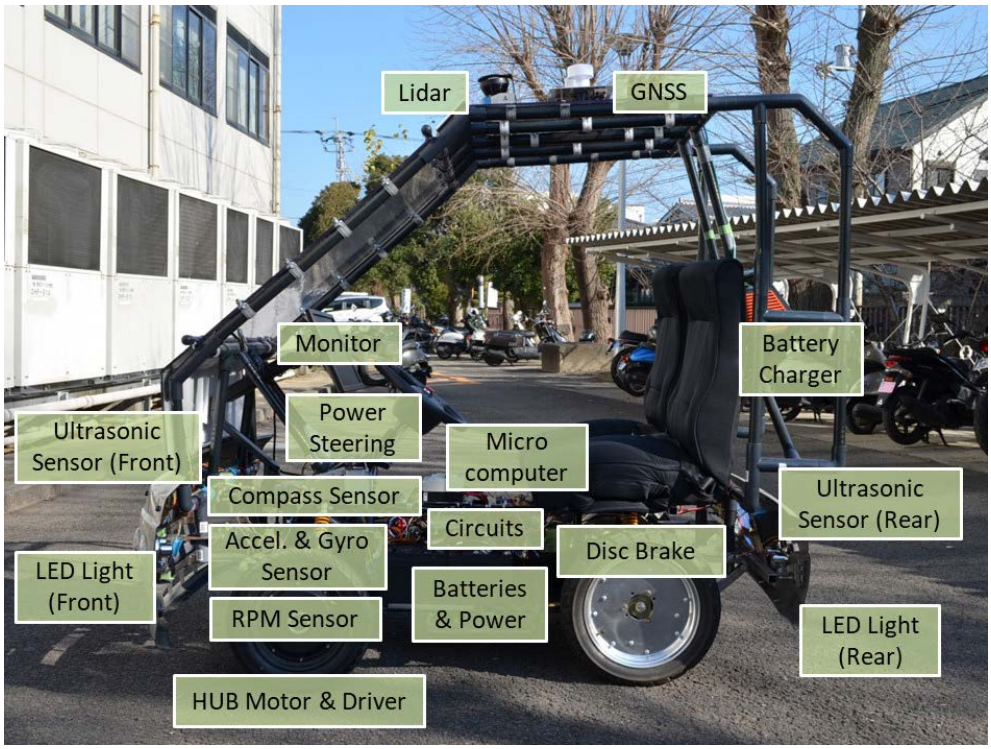

Figure 3.2: Parts configuration and installation

3.1.2 Battery System

Figure 3.3 shows a diagram of battery-powered electric system of the vehicle. DC 48 V and 12 V batteries are installed at the chassis bottom. 48 V battery is assembled by 12 V batteries 4ea in series. 48 V battery is charged by AC 100 V battery charger. 12 V battery is charged 48 V to 13 V DC-DC converter. 5 V and 3.3 V are generated by 12 V to 5 V, 5 V to 3.3 V DC-DC converter. 48 V battery supplies power to Hub-motors. 12 V battery supplies power to power steering, disc brake, lidar and LED lights. 5 V and 3.3 V supply to circuits.

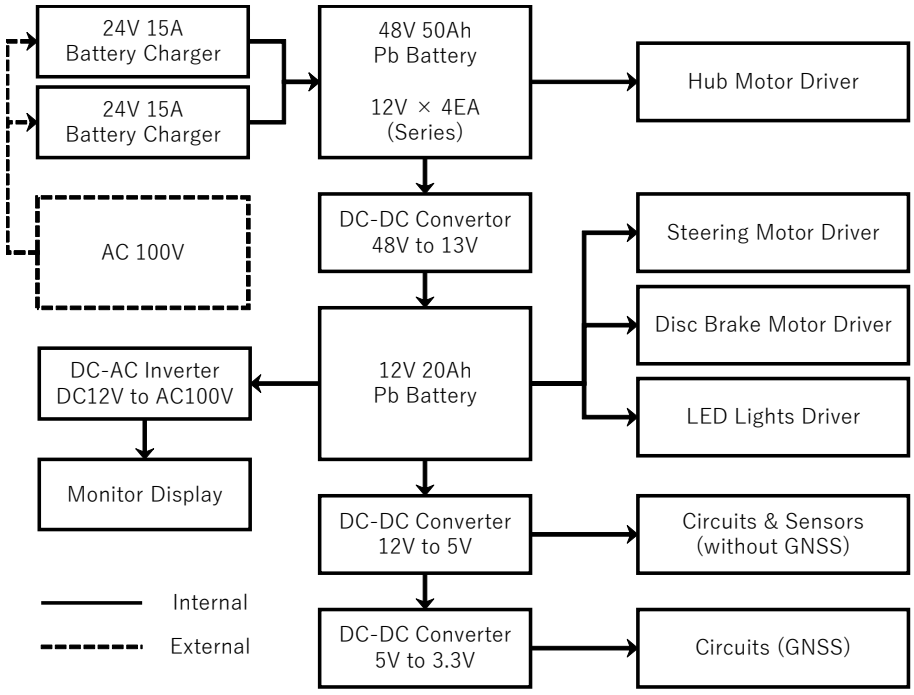

Figure 3.3: Battery power system

3.1.3 Communication Configuration

Figure 3.4 shows a diagram for vehicle communication configuration. The main communication protocol is CAN. CAN communication is the most popular internal communication for vehicle. Each device transmits its data to CAN bus. CAN bus speed is 1 Mbps. All messages are updated 0.1 sec. Lidar is communicated by TCP/IP protocol with a microcomputer. I2C communication is used for digital compass, ultrasonic, gyro, accelerometer, RPM sensor. GNSS module is connected by UART serial communication. Every device transmits diagnostic message to UART port.

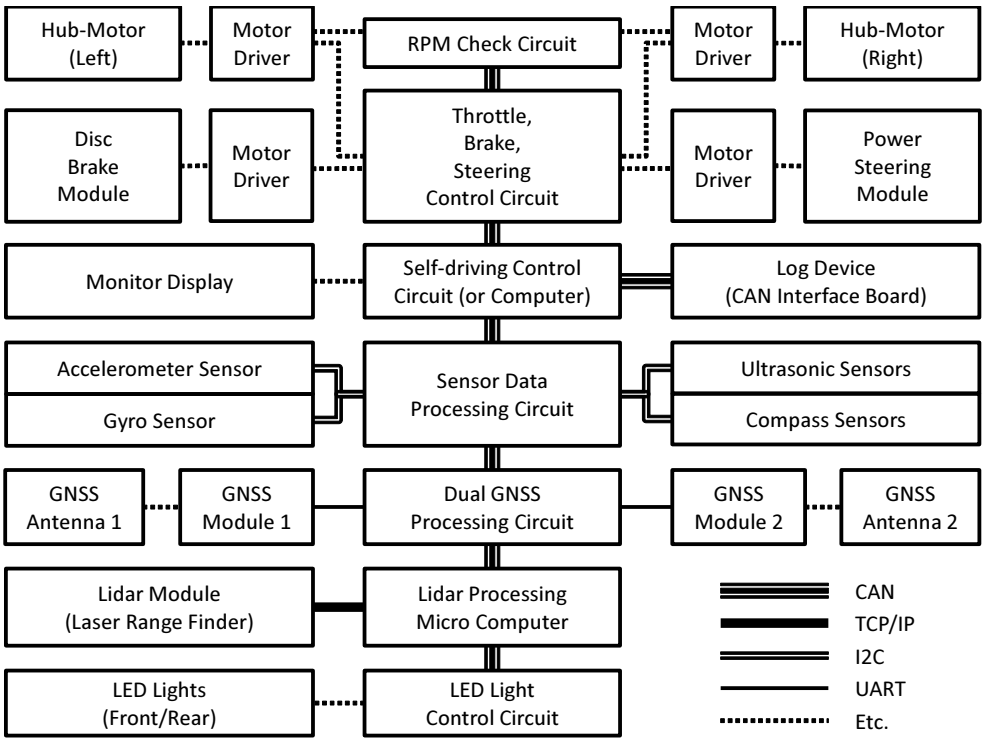

Figure 3.4: Communication configuration

3.1.4 Microprocessor and Microcomputer

AT90CAN128 microprocessor and BeagleBoneBlack microcomputer are used for the main processing unit of vehicle. AT90CAN128 and BeagleBoneBlack include Full-CAN communication driver. AT90CAN128 is used for control or sensor circuits. BeagleBoneBlack is used for lidar data query and processing.

3.1.5 Hub-Motor with Hole Sensors

Two 48 V 1 kW 3 phase hub-motors are power train of the vehicle. Hub-motor is installed at front left and right wheels. Hole sensor is included in the Hub-motor. A total 72 pulses are generated in one rotation. RPM is calculated by hole sensor pulse. Motor driver input is 0 to 5 V analog signal.

3.1.6 Software Differential for Front-wheels

In the situation of vehicle turning, in order to minimize drive resistance that is occurred by speed unbalance between inside wheel and outside wheel, software differential is applied on throttle control circuit. When the vehicle drives straight, input voltage level of two hub-motor is equal. When the vehicle turns, input voltage level of inside wheel is lower than straight situation. Also, input voltage level of outside wheel is higher than straight situation.

3.1.7 Dual Brake System

Regeneration brake and disc brake are applied in the vehicle for deceleration and stop. Regeneration brake is included in the hub-motor. Analog input voltage determines regeneration brake force. Disc brake is installed at the rear wheel. Disc brake is actuated by motor and Pulse Width Modulation(PWM) signal. During the self-driving, the brake is automatically controlled. However, a manual brake is still available. If automatic brake signal and manual brake signal are simultaneously inputted, brake motor is actuated by more deep brake signal [60]-[63].

3.1.8 Motor Powered Steering

In order to change vehicle direction by automatic, 12 V 350 W power steering motor is installed in the steering wheel axis. Motor is controlled by PWM signal. Steering wheel angle is measured by potentiometer [64],[65].

3.1.9 Dual GNSS Module

Dual GNSS antenna and module is installed on the roof. Figure 3.5 shows GNSS antennas and modules. GNSS antenna SANNAV DS-56, GNSS module u-blox CAM-M8C is applied for positioning system. Weighted averaging correction for positioning is implemented by dual GNSS.

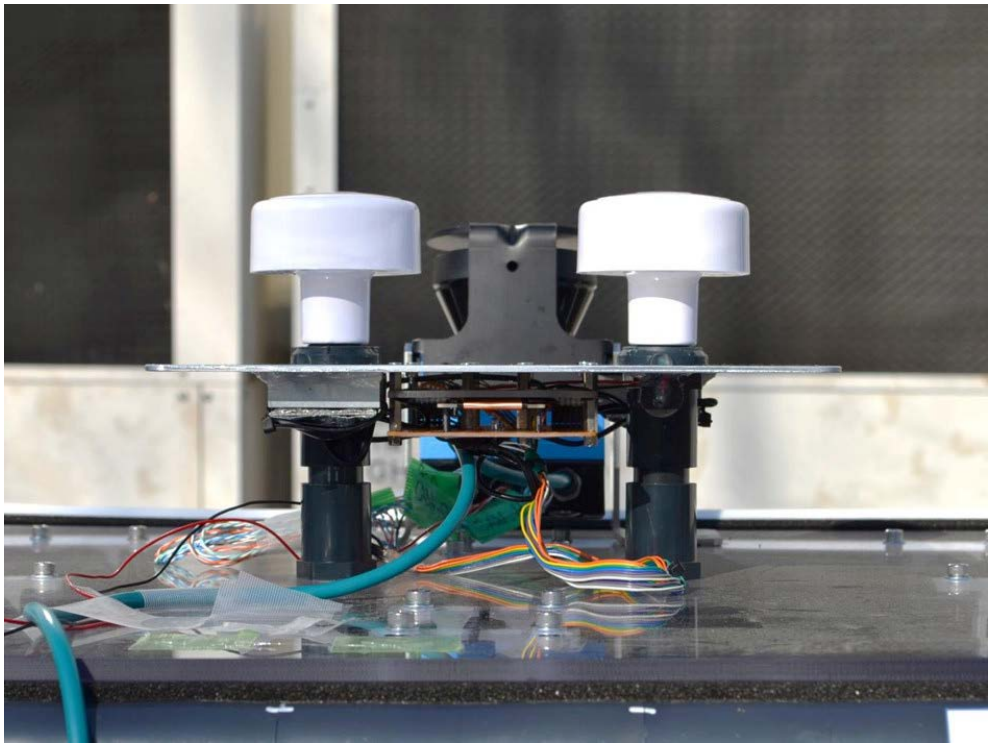

Figure 3.5: Dual GNSS antenna and module

3.1.10 Lidar Sensor

Figure 3.6 shows a LMS100 lidar (or laser-range-finder) sensor by SICK. Lidar sensor detects wide area obstacle. Lidar is installed at the roof top of the vehicle. Maximum detection distance is approximately 20 m, Maximum detection angle is approximately 270 degree, resolution is 0.5 degree.

3.1.11 Ultrasonic Sensor

In order to detect near area obstacles, ultrasonic sensors are installed on the front bumper and rear bumper. The installation is shown in Fig. 3.7. Maximum detection distance is approximately 6 m. Update frequency is 10 Hz.

Figure 3.6: Lidar sensor

Figure 3.7: Arrangement of ultrasonic sensors

3.1.12 Dual Digital Compass Sensor

Dual digital compass is installed at front of vehicle for measuring heading angle. Digital compass outputs the north as 0, east as 900, south as 1800, west as 2700. Resolution is 0.1 degree.

3.1.13 LED Light for Human Machine Interface

In order to indicate vehicle status and driving status to humans, full color LED is installed at front bumper and rear bumper. Figure 3.8 shows blue color turned on vehicle. In normal situation, front day time running light (DRL) is turned on. When the brake is pushed, red light is turned on in the rear lights. When obstacles are detected, all lights are turned to red and blink. After vehicle is clearly stopped, the lights are turned to green for waiting and during the pedestrian escape.

Figure 3.8: Full color LED lights

3.1.14 Characteristics of Compact Vehicle

Table 3.1 indicates physical specification of the developed compact vehicle. The vehicle is geometrically similar with light-weight small car.

Table 3.1: Physical specification of compact vehicle

Parameter	Unit	Value
Wheelbase	mm	970
Front Axle-distance Centroids	mm	390
Rear Axle-distance Centroids	mm	580
Body Width	mm	1260
Body Length	mm	2000
Body Height	mm	1630
Empty Vehicle Weight	kg	300
Maximum Speed	km/h	45
Maximum Instantaneous Acceleration	m/s^2	1.2
Maximum Steering Angle	deg.	30
Minimum Turning Radius	mm	2000

Figure 3.9 shows a graph of acceleration characteristic of the vehicle. Approximately 10 sec is needed to reach for 20 km/h.

Figure 3.10 shows a graph of vehicle braking characteristic. When brake starts, approximately 30 km/h, a braking distance is need of approximately 5 m.

The maximum steering angle is left 40 degree, right 40 degree, which total to 80 degree mechanically. However, for driving safety, maximum steering angle is limited at left 30 degree, right 30 degree, which total to 60 degree by the software.

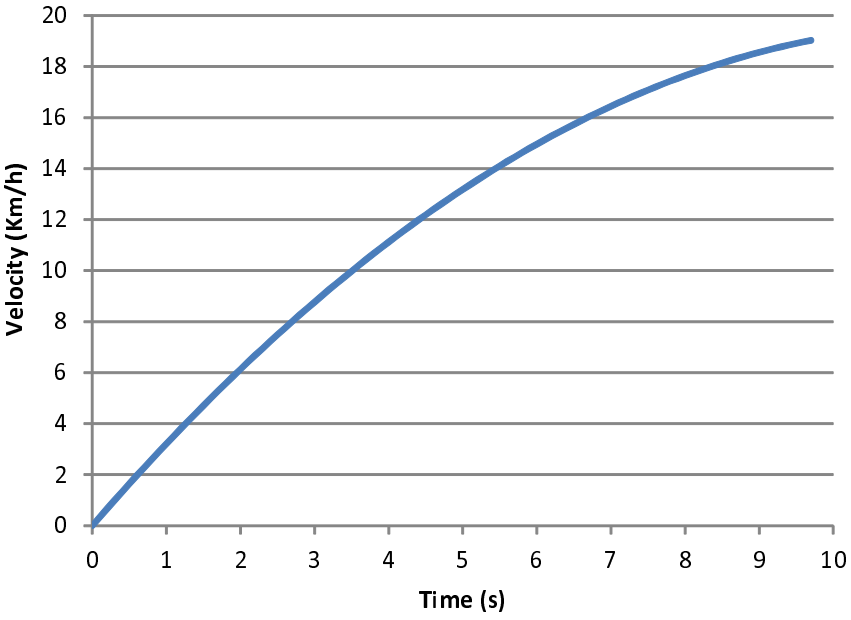

Figure 3.9: Characteristic of acceleration

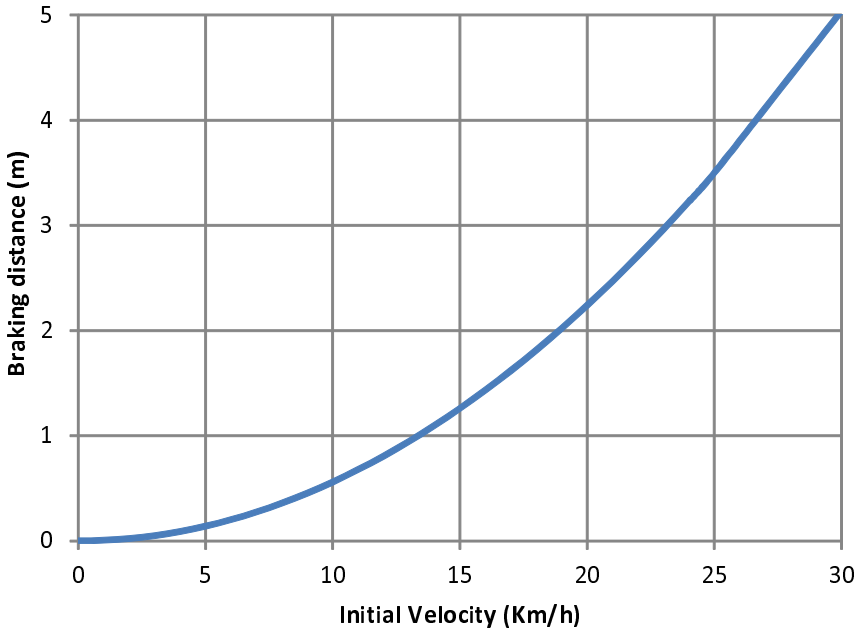

Figure 3.10: Characteristic of braking

3.2 Small-scale Vehicle Development

Figure 3.11 shows an appearance of constructed small-scale vehicles implemented for the proposed semi-self-driving system. In the experiment, the vehicle A is used for preceding vehicle, while B and C are used for following the vehicle. The vehicle is constructed by a main circuit, a GNSS antenna, a GNSS receiver module, a digital compass, servo motors for the steering wheel and throttle control, a DC motor for driving wheels, a DC motor driver and a 7.2V Ni-MH battery. The main circuit is constructed by a microprocessor, wireless communication module and power supply. Configuration of the preceding vehicle and following vehicles are the same [66].

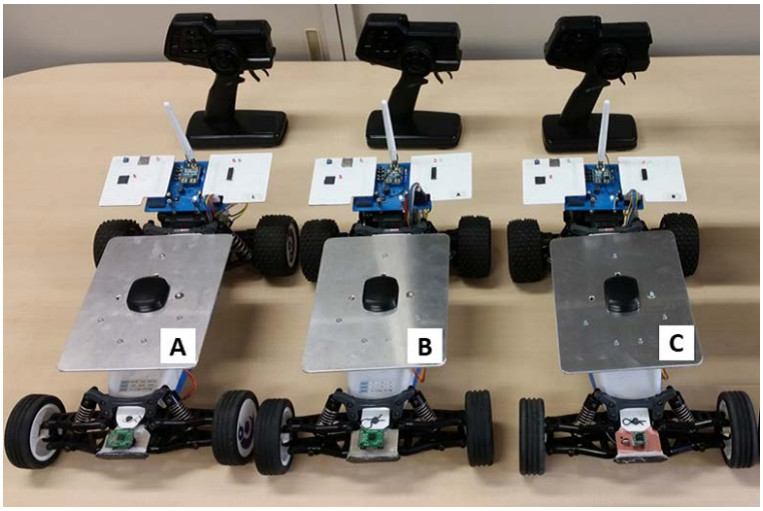

Figure 3.11: Constructed small-scale vehicles

Figure 3.12 shows a hardware configuration. The GNSS active antenna (SAN JOSE DS-28) is installed on the aluminum roof of the body. The GNSS receiver module (u-blox CAM-M8) based on u-blox M8 chipset is performed with 5 Hz position updating cycle. The digital compass module (HONEYWELL HMC6352) has a precise performance of 0.1 degree increments. For the wireless communication module, MAX STREAM XBee Pro is installed. Communication distance of the module is approximately 1 km under the clear channel condition. The microprocessor (ATMEL Atmega64L) calculates the vehicle speed and steering angle. Position and status of the vehicles are transmitted to following vehicle and the monitoring PC, simultaneously.

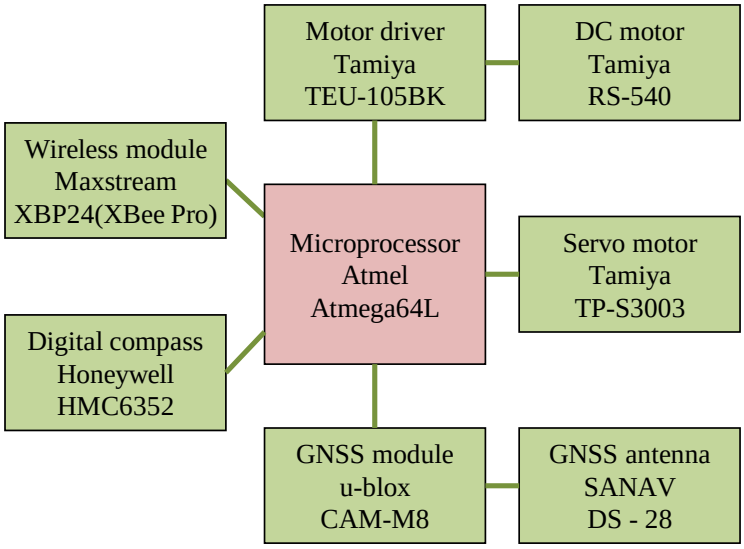

Figure 3.12: Hardware configuration of the small-scale vehicle

Table 3.2 indicates the physical specifications of the small-scale vehicle. Acceleration characteristic would be changed by battery condition. Brake is not installed on the vehicle.

Table 3.2: Physical specification of small-scale vehicle

Parameter	Unit	Value
Wheelbase	mm	290
Front Axle-distance Centroids	mm	200
Rear Axle-distance Centroids	mm	90
Body Width	mm	240
Body Length	mm	400
Body Height	mm	135
Empty Vehicle Weight	kg	2
Maximum Speed	km/h	20
Maximum Steering Angle	deg.	45
Minimum Turning Radius	mm	680

Chapter 4

Experiment of Self-driving System

4.1 Experiment of Single Mode Self-driving

4.1.1 Setup for Test

Figure 4.1 shows a ring-type route for single mode self-driving test. Ring-type route is geometrically similar with square. Target velocity is set to 5 km/h. When the vehicle arrives at its final destination, a temporary destination is reset to initial way point. Figure 4.2 shows a one-way type route for testing. When the vehicle arrives at its final destination, self-driving is terminated in one way route test. Target velocity is also set to 5 km/h. All of GNSS coordinates of the current positions are corrected by using a multiple GNSS method. The correction method is detailed in the chapter 5.

4.1.2 Experiment Result

Single mode self-driving result on the ring type route is indicated in Fig. 4.3. Route tracking algorithm was normally operated during experiment. However, position errors are caused by GNSS module and steering angle error is caused by digital compass calibration imperfection. Before the next experiment, digital compass was re-calibrated by forced calibration procedure. Single mode self-driving result on the one way type route is indicated in Fig. 4.4. Route tracking algorithm was also normally operated during experiment. Position errors were remarkably less than ring type route test.

Figure 4.1: Setup for ring type route

Figure 4.2: Setup for one way type route

Figure 4.3: Self-driving result in ring type route

Figure 4.4: Self-driving result in one way route

4.2 Experiment of Platooning Mode Self-driving

4.2.1 Setup for Tracking and Approaching Test

Environment

Figure 4.5 shows the experimental environment where a track is constructed in the form of vertical and horizontal 20 m square, and each corner and the center position are marked with orange rubber corns. The experiment was carried out on the ground under the sunny day with open sky condition. Here, the digital compass was calibrated before the experiment. The vehicle for platooning mode self-driving depends on only a relative GNSS coordinate for the positioning, without a position correction method.

Procedure of the Tracking Test

The preceding vehicle is manipulated to the point 1-2-3-4-1 constant velocity. The following vehicle automatically drives with tracking to the preceding vehicle continuously. Trajectory of each vehicle is recorded by the monitoring server.

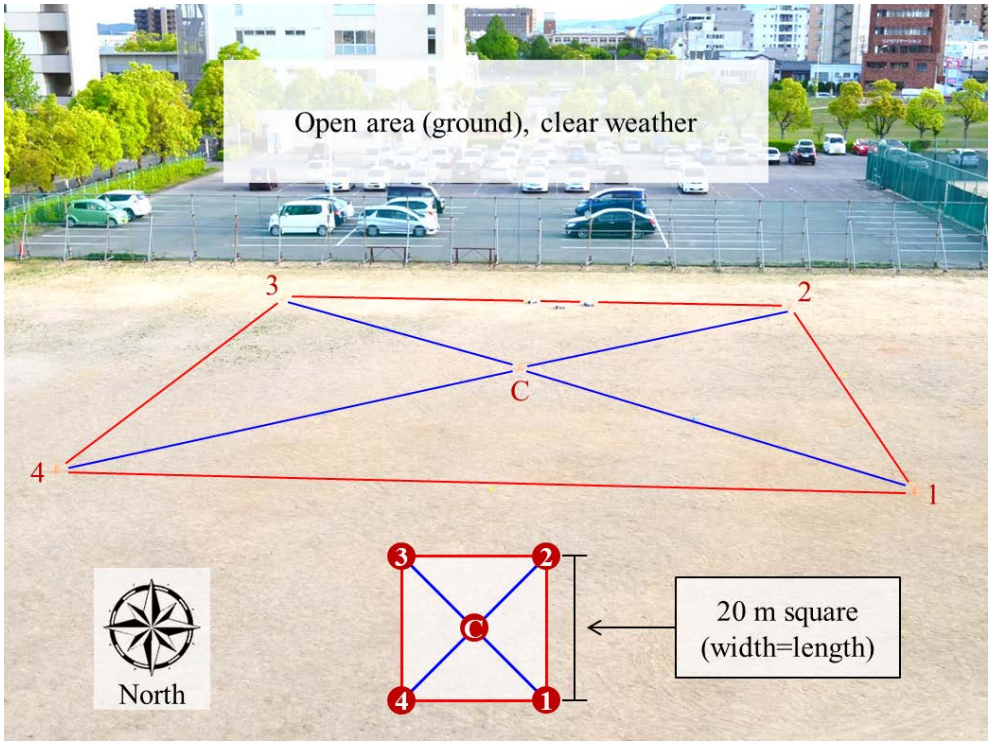

Figure 4.5: Experimental environment and track setting

Procedure of the Approaching Test

First, the first following vehicle drives with tracking to the preceding vehicle, and the second following vehicle tracks to the first following vehicle. Second, the preceding vehicle stops on the center point of the track. If the relative distance under the GNSS data is shorter than 30 cm, following vehicles are immediately stopped. At that situation, the actual relative distance is measured. An example of actual relative distance measurement is shown in Fig. 4.6. The reference of the measurement is at the center of the GNSS antenna on vehicle. Simultaneously, relative distance by the GNSS is recorded by a monitoring server. The position error is calculated by these two distances. The experiment was repeated for 10 times.

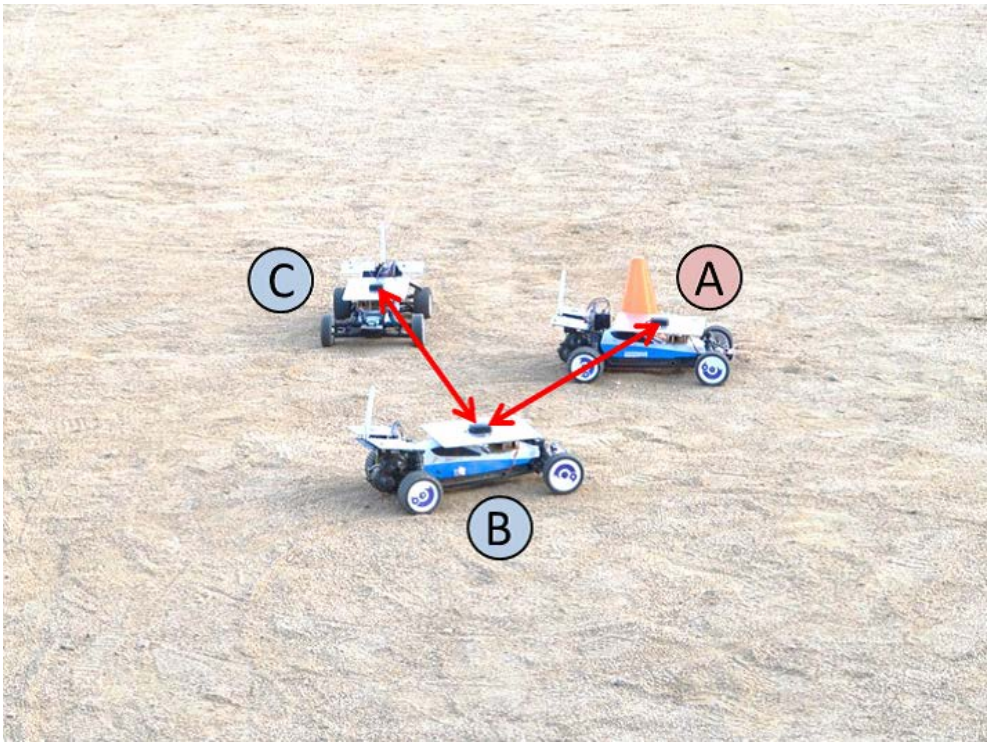

Figure 4.6: Measurement of actual distance in approaching test

4.2.2 Setup for Position Error Measurement Test

Environment

In order to setup the reference absolute position, a triangular point is used in position error measurement. The triangular point is located on the mountain Bizan in the Tokushima prefecture in JAPAN. Figure 4.7 shows the triangular point. The measurement was carried out under the clear whether with open sky condition.

Figure 4.7: Triangular point in the Tokushima prefecture, JAPAN

Procedure of Position Error Measurement

Figure 4.8 shows the setup of position error measurement. The vehicle A is allocated on the center of the triangular point. The other vehicle is allocated on 5 m away point from the triangular point. Positions of both vehicles are measured for 3 hours. The position error is calculated by one dimension Root Mean Square(RMS) method [67]. It is possible to evaluate the accuracy of relative position.

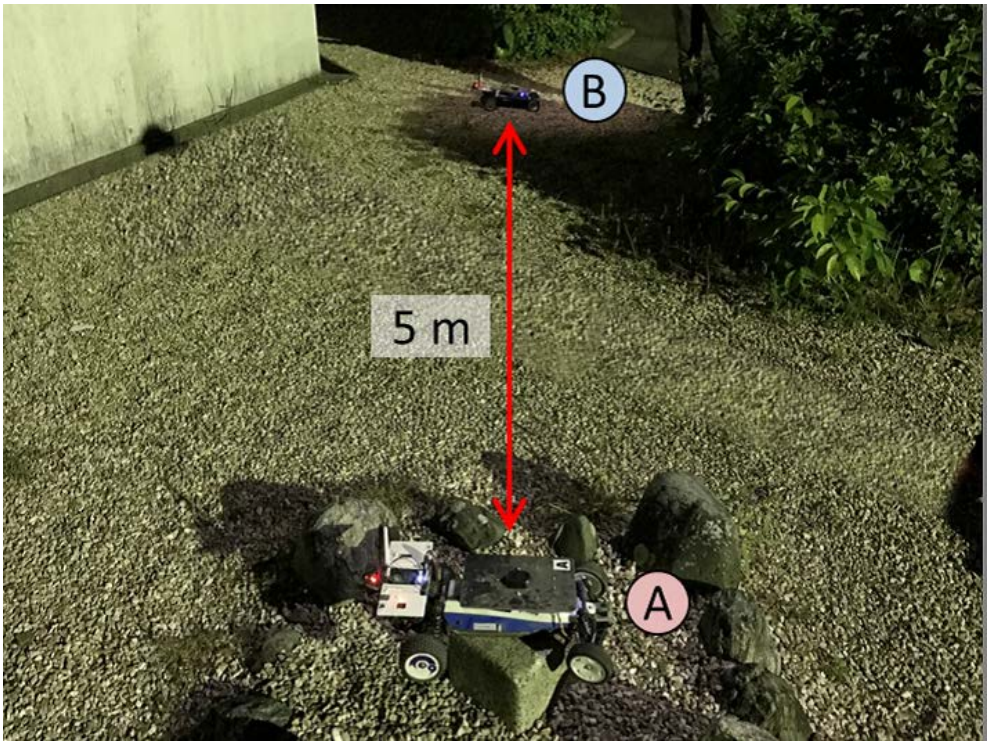

Figure 4.8: Position error measurement

4.2.3 Experiment Result

Tracking Test

Figures 4.9 and 4.10 show the tracking performances for the moving preceding vehicle. The following vehicle B could track on the trajectory of the moving preceding vehicle A under the GNSS data. However, it is noted that the absolute trajectory has positioning errors more or less than 100 cm against the GNSS data.

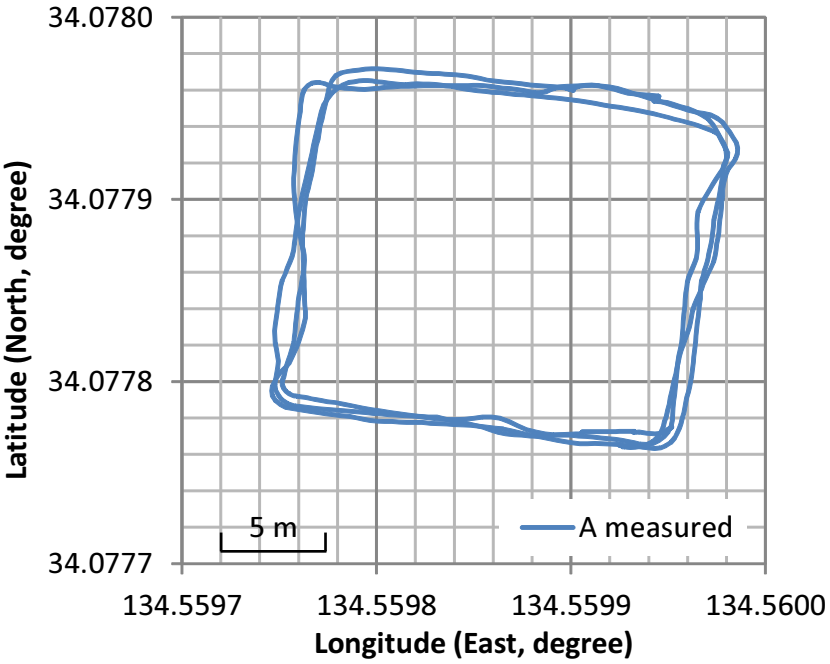

Figure 4.9: Trajectory of the preceding vehicle in the tracking test

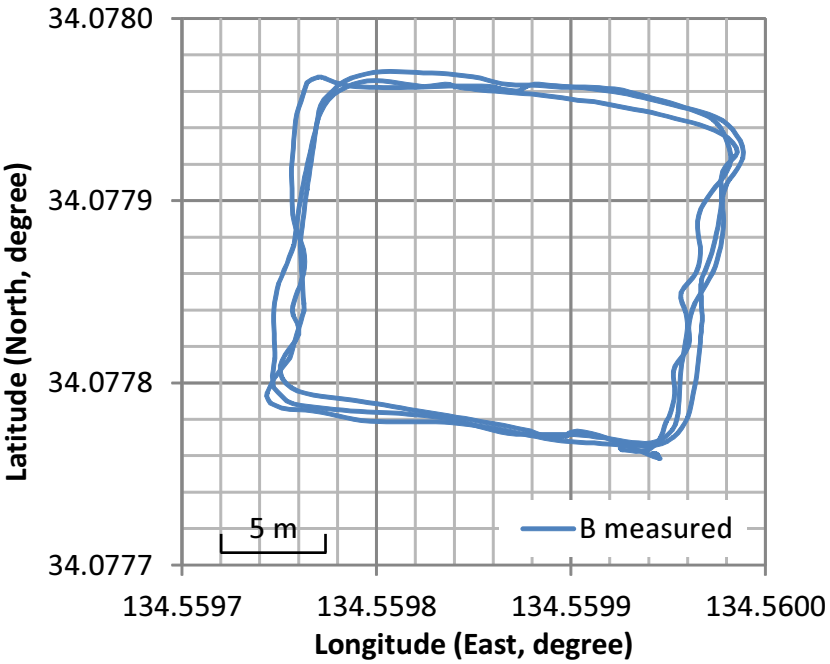

Figure 4.10: Trajectory of the following vehicle in the tracking test

Approaching Test

Position errors between the relative distance calculated by the GNSS and the actual relative distance for each test are listed in Table 4.1. Maximum, minimum and average distance errors between the preceding vehicle as A and the first following vehicle as B are 54 cm, 0 cm, and 29.8 cm, respectively. Maximum, minimum and average distance errors between the first following vehicle as B and the second following vehicle as C are 54 cm, 3 cm, and 30.4 cm, respectively. Test results for the two cases are similar to each other. Note that the test was conducted under the GNSS receiving status which HDOP is approximately 0.6.

Table 4.1: Position errors of approaching test

Test No.	$\overline{AB}$ GNSS	$\overline{BC}$ GNSS	$\overline{AB}$ Actual	$\overline{BC}$ Actual	$\overline{AB}$ Error	$\overline{BC}$ Error
1.	70 cm	104 cm	32 cm	60 cm	38 cm	44 cm
2.	14 cm	91 cm	68 cm	88 cm	54 cm	3 cm
3.	72 cm	30 cm	60 cm	84 cm	12 cm	54 cm
4.	40 cm	23 cm	40 cm	76 cm	0 cm	53 cm
5.	49 cm	40 cm	100 cm	36 cm	51 cm	4 cm
6.	72 cm	80 cm	99 cm	105 cm	27 cm	25 cm
7.	79 cm	85 cm	44 cm	43 cm	35 cm	42 cm
8.	96 cm	57 cm	95 cm	42 cm	1 cm	15 cm
9.	94 cm	18 cm	65 cm	41 cm	29 cm	23 cm
10.	86 cm	21 cm	35 cm	62 cm	51 cm	41 cm
Minimum error					0 cm	3 cm
Maximum error					54 cm	54 cm
Average error					29.8 cm	30.4 cm
Average HDOP					0.614	0.617

Position Error Measurement

Figures 4.11, 4.12 and Table 4.2 show the measurement results of the position error. Average position error in independent measurement is approximately 160 cm. On the other hand, the average position error in relative measurement is decreased to 53 cm (-68.8%). The RMS 1σ means that 68.3% position errors are occurred smaller than

the 1σ value. The RMS 1σ error is approximately 215 cm in independent mode, and 98 cm (-54.4%) in relative mode. The RMS 2σ means that 95.5% position errors are occurred smaller than the 2σ value. The RMS 2σ error is approximately 266 cm in independent mode, and 139 cm (-47.7%) in relative mode. From these result, significant improvement of the GNSS position accuracy has confirmed in the relative positioning mode.

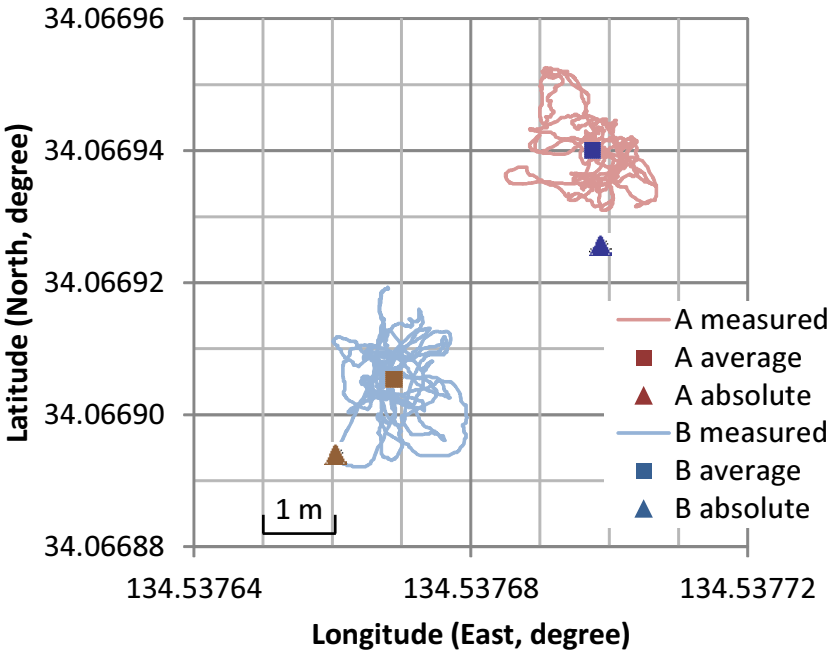

Figure 4.11: Result of the position error measurement

Table 4.2: RMS error of the measurement

Type	Mean	RMS 1σ	RMS 2σ
Independent (A)	163 cm	224 cm	279 cm
Independent (B)	157 cm	207 cm	254 cm
Relative (A,B)	53 cm	98 cm	139 cm

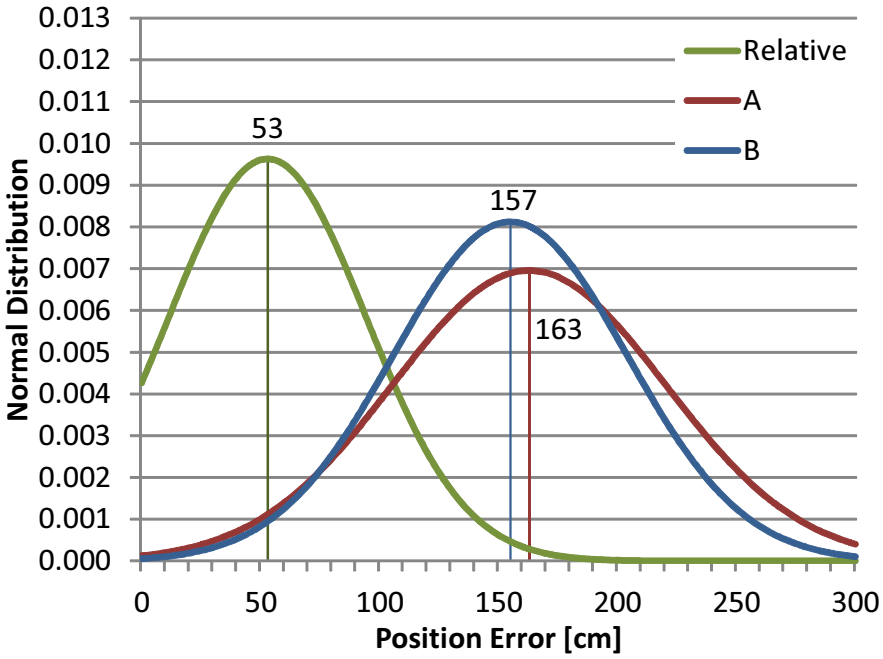

Figure 4.12: Normal distribution of the measurement result

4.3 Experiment of Collision Prevent Algorithm

Figures 4.13 and 4.14 show the experiment of collision prevention stop and resume function. Target vehicle velocity is set to 5 km/h. Stopping test is conducted with 4 patterns. Pattern 1 was standing in front of vehicle. Pattern 2 was walking close to the front of bumper from the front of vehicle. Pattern 3 was walking close to the front of bumper from the vehicle side. Pattern 4 was at random interference.

Figure 4.13: Stop test for collision prevention 1

Figure 4.14: Stop test for collision prevention 2

4.3.1 Experiment Result

Table 4.3 shows test result of stop for collision prevention. O means success, X means fail. In a situation of standing front of the vehicle, stopping and collision prevention has 100 % succeed. In other situations, stopping has succeeded all time. However collision has succeeded 80 % to 90 %. That was the reason why, when the obstacle approached very suddenly from a very close position to the vehicle, speed reduced time and braking distance was insufficient. The result means the stop zone is necessary to extend wider.

Table 4.3: Test result of stop for collision prevention (O: Success, X: Fail)

Test No.	Standing at the front		Walking from front		Walking from side		Random	
	Stop	Collision	Stop	Collision	Stop	Collision	Stop	Collision
1	O	O	O	O	O	X	O	O
2	O	O	O	O	O	O	O	O
3	O	O	O	O	O	O	O	O
4	O	O	O	O	O	O	O	X
5	O	O	O	O	O	O	O	O
6	O	O	O	X	O	O	O	O
7	O	O	O	O	O	X	O	O
8	O	O	O	O	O	O	O	O
9	O	O	O	O	O	O	O	O
10	O	O	O	O	O	O	O	X
Total	100 %	100 %	100 %	90 %	100 %	80 %	100 %	80 %

Chapter 5

Proposed Correction Algorithms

5.1 Position Correction by Learning Algorithm

This section shows a novel improvement method of position identification accuracy by using multiple GNSS units which consist of several fixed stations, a vehicle, and a hierarchical neural network (HNN). The input information of the HNN is a relative distance between each GNSS unit. The HNN corrects the position of vehicle based on the information of fixed GNSS stations.

Figure 5.1 shows the concept of this research. In this concept, there are a number of vehicles which have a GNSS unit for each and several fixed point GNSS stations. Then each vehicle knows the estimated their position by using corrected information obtained from fixed GNSS station. In this system, the price of each GNSS unit is kept low since the each GNSS has poor precision performance. However, all of GNSS units make a sensor network to improve the position identification accuracy. It realizes the production of the low cost vehicle and promotes the introduction of highly reliable platooning system.

To learn the HNN, a typical back propagation (BP) algorithm was used which is often used as a learning algorithm of the HNN. The BP algorithm intends to decrease the error function E defined as follows:

$$E = \frac{1}{2}\left\{(X_{m1}^{HNN} - X_{m1}^{T})^2 + (Y_{m1}^{HNN} - Y_{m1}^{T})^2\right\} \tag{5.1}$$

where X_{m1}^{T} is the supervised data of x component, and Y_{m1}^{T} is the supervised data of y

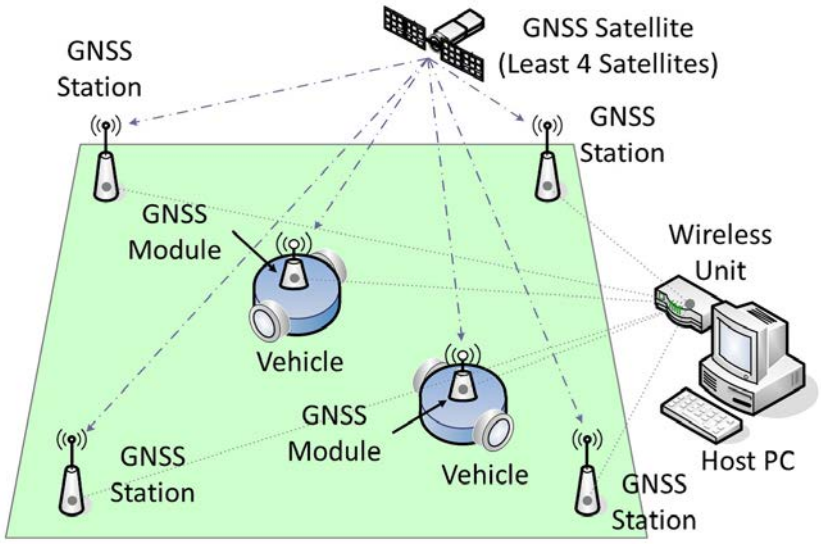

Figure 5.1: Concept of position identification improvement system by GNSS network

component. Then the connection weights of the HNN are adjusted by as follows:

$$(\Delta w_{ji}, \Delta w_{kj}) = \left(\frac{\partial E}{\partial w_{ji}}, \frac{\partial E}{\partial w_{kj}} \right) \tag{5.2}$$

where Δw_{ji} is the correction value of the neuron between hidden layer's neuron j and input layer's neuron i, and Δw_{kj} is the correction value of the neuron between output layer's neuron k and hidden layer's neuron j.

5.1.1 Measurement Condition

Figure 5.2 and Figure 5.3 show the arrangement of each GNSS unit. The fixed point GNSS stations are located at corners on a reference path, P1 (x_{p1}, y_{p1}), P2 (x_{p2}, y_{p2}), P3 (x_{p3}, y_{p3}), and P4 (x_{p4}, y_{p4}). And the small-scale vehicle, M1 (x_{m1}, y_{m1}), automatically control the moving speed at approximately 2.25 m/s constant. The reference path is set at approximately 20 meters square feet. The experiment was conducted on ground, as shown in Figure 5.3, where the an environment has flat surface and open sky. It is good condition for receiving the signal from GNSS satellites. All GNSS data of fixed stations and vehicle are collected by the host computer to calculate the information of position correction value. Here, sampling time is set to 1.0 s for the position data acquisition and the data communication.

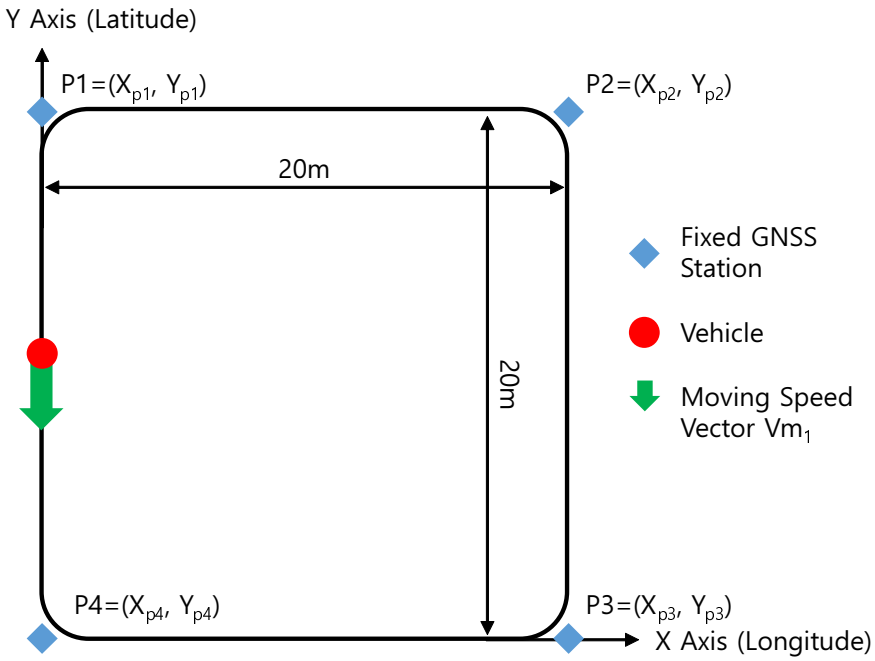

Figure 5.2: Experimental condition: Relationship of each GNSS unit

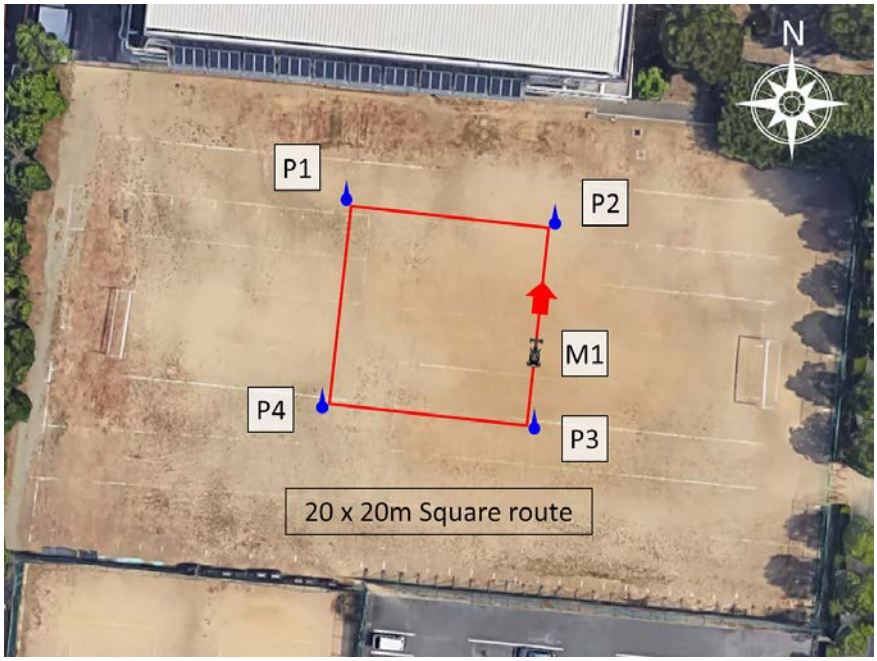

Figure 5.3: Experimental condition: Ground, Open sky

5.1.2 Measurement Result

The measurement results of each GNSS unit are shown in Figure 5.4. The X and Y axis indicate a longitude and latitude, respectively. The figure shows approximately 30 meters wide and 30 meters long. From this figure, although all fixed point GNSS stations do not move but stay still, the data of the fixed point GNSS station was tend to disperse widely at certain area. In addition, they do not indicate the same dispersion performance and also, the orbit data of the small-scale vehicle which moved around on the route 20 meters square does not exactly indicate its orbit and it is far from accurate data.

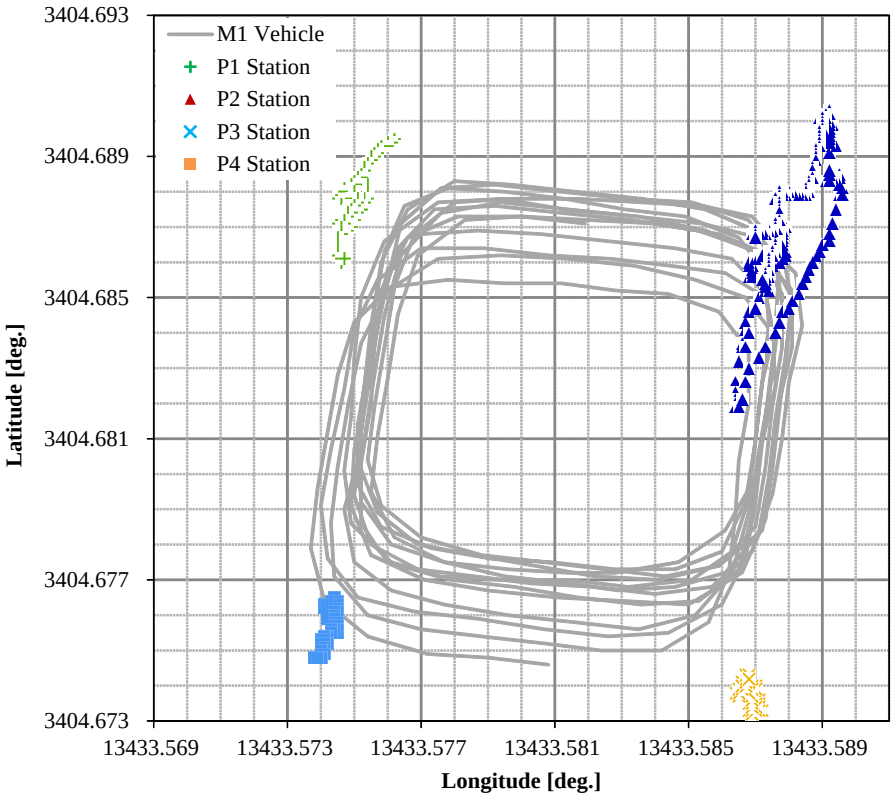

Figure 5.4: Measured positions of each GNSS unit

5.1.3 Correction Simulation

From the measurement results, I confirmed that the dispersion of obtained GNSS units data has non-linear characteristics. Therefore we consider to use a hierarchical neural network (HNN) which is good at treating non-linear data and pattern space in order to improve the measurement accuracy. The position error of GNSS data is caused by a variety of factors surrounding a GNSS unit. Here, the obtained GNSS position data $\mathbf{P}_n$ is defined as follows:

$$\mathbf{P}_n = \mathbf{P}_n^G + \mathbf{\Delta} + \delta_n \tag{5.3}$$

where $\mathbf{P}_n^G$ is the precise value without error, $\mathbf{\Delta}$ is the common error of GNSS module, and δ_n is the individual variability of GNSS module. From Equation (5.3), we can compensate for the common error $\mathbf{\Delta}$ by subtracting the output position data of each GNSS unit (ex. $P_1 - P_2$). In addition, if the position of the fixed point GNSS station is already known, the individual variability factor δ_n is finally derived. It is useful way mentioned above to estimate exact location of the fixed point GNSS station. However it can not apply to a GNSS module of a vehicle. Because the position of a vehicle usually moves around. Therefore I propose a position correction system of a vehicle by using a HNN based on the information of the fixed point GNSS station.

Figure 5.5 shows the configuration of the proposed position correction system of the vehicle. The parameters of the HNN are indicated in Table 5.1. At first, the system calculates the relative distance (e.x. $x_{p1} - x_{pn}$, $y_{p1} - y_{pn}$) in vector quantity of each GNSS station which is between the fixed point GNSS station P1 and the other stations Pn (n=2, 3, 4, 5), including the vehicle M1. After that the relative distance values are inputed to the HNN. And the HNN outputs estimated position of the vehicle M1 (x_{m1}, y_{m1}).

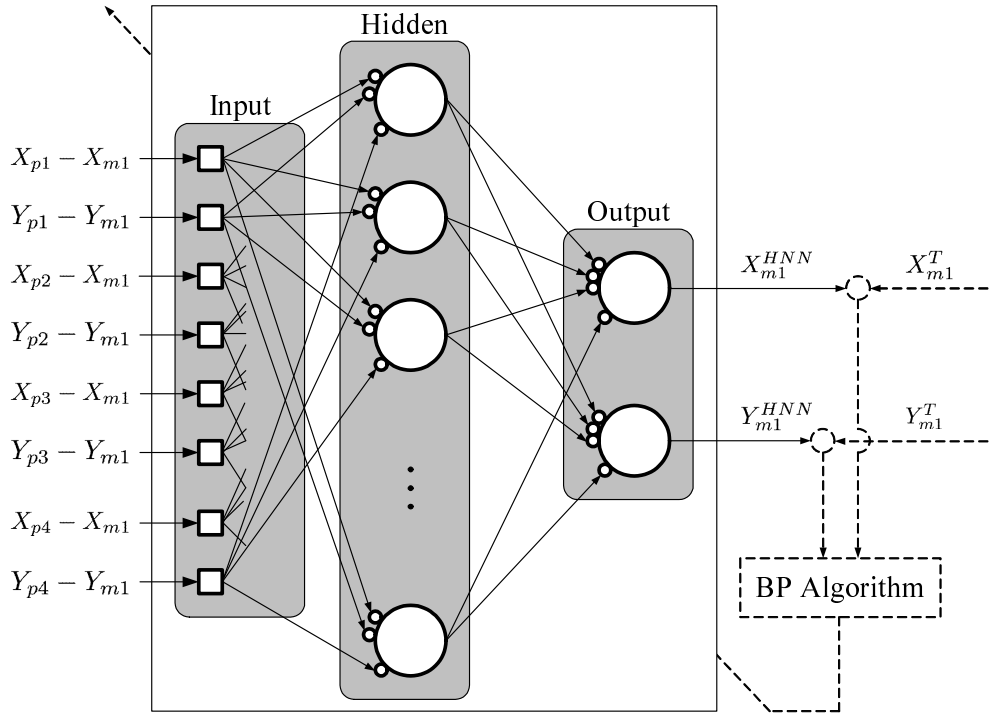

Figure 5.5: Proposed position correcting system using HNN

Table 5.1: Parameters of HNN

The number of neuron			Learning	
Input	Hidden	Output	coefficient	Iteration
8	8	2	0.01	1000

5.1.4 Learning Result of the HNN

Figure 5.6 shows the transition of a root mean square error ($RMSE$) defined by Equation (5.4) during the learning process. In Equation (5.4), N is the number of samples, X_{m1}^{HNN} and Y_{m1}^{HNN} are the estimated longitude and latitude by the HNN, X_{m1}^{T} and Y_{m1}^{T} are the actual longitude and latitude. After the number of iteration was over approximately 800, the $RMSE$ of the HNN has been almost converged to the constant value, $RMSE = 0.06$.

$$RMSE = \sqrt{\frac{\sum^{N}\{(X_{m1}^{HNN} - X_{m1}^{T})^2 + (Y_{m1}^{HNN} - Y_{m1}^{T})^2\}}{N}} \tag{5.4}$$

Figure 5.7 shows the teaching data of the actual reference path and fixed point positions. The learning result of the HNN is shown in Figure 5.8. From Figure 5.8, we can see that the observed data of the vehicle has been dramatically converted and fitted to the actual orbit of the vehicle by the HNN. Moreover, Figure 5.9 shows time variations of the position error between the actual orbit and the estimated position of the vehicle during several times go-around. It seems that the error changes periodically. Finally, Figure 5.10 shows the average, minimum and maximum error between actual orbit and estimated position of vehicle. Average error, minimum error, maximum error are improved approximately 16.91%, 47.45%, 4.43%, respectively.

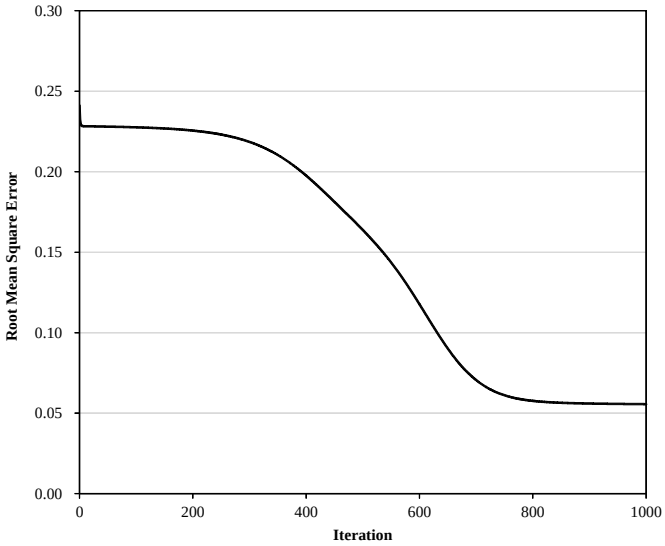

Figure 5.6: Transition of $RMSE$ while HNN was learning

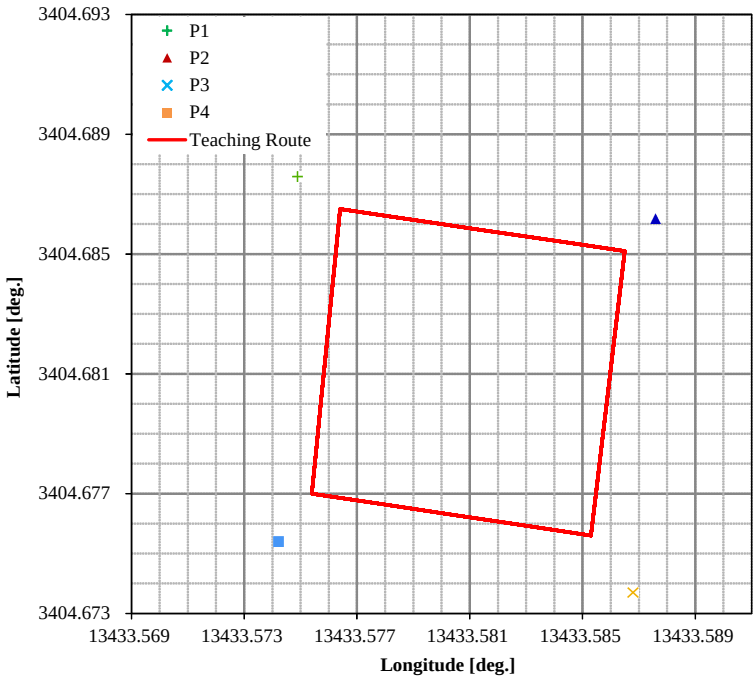

Figure 5.7: Teaching data : actual route and positions

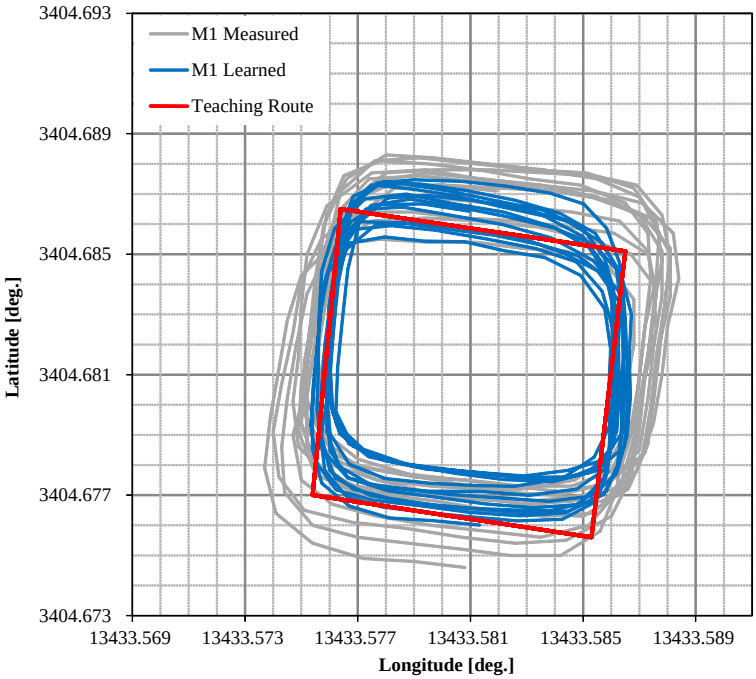

Figure 5.8: Learning result of HNN expressed on X-Y coordinate

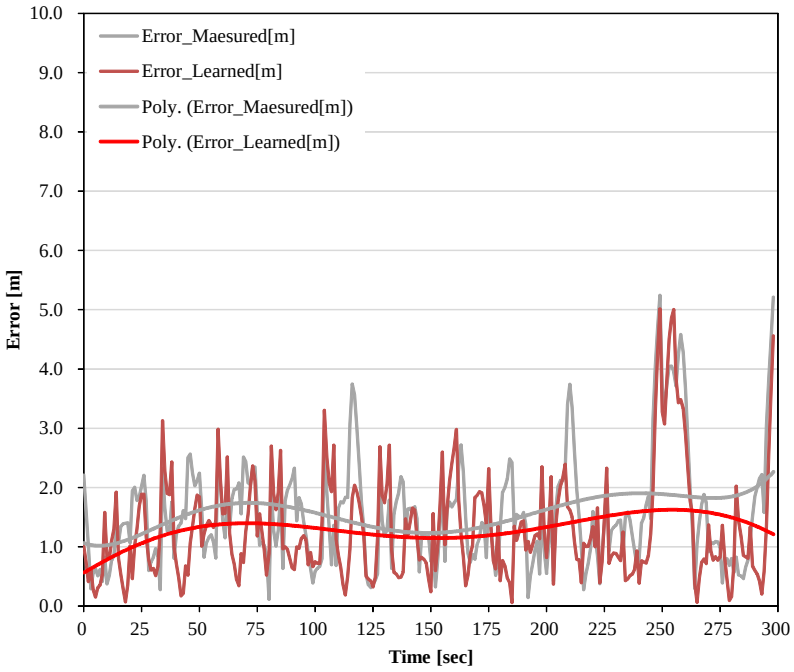

Figure 5.9: Error between actual orbit and estimated position of vehicle

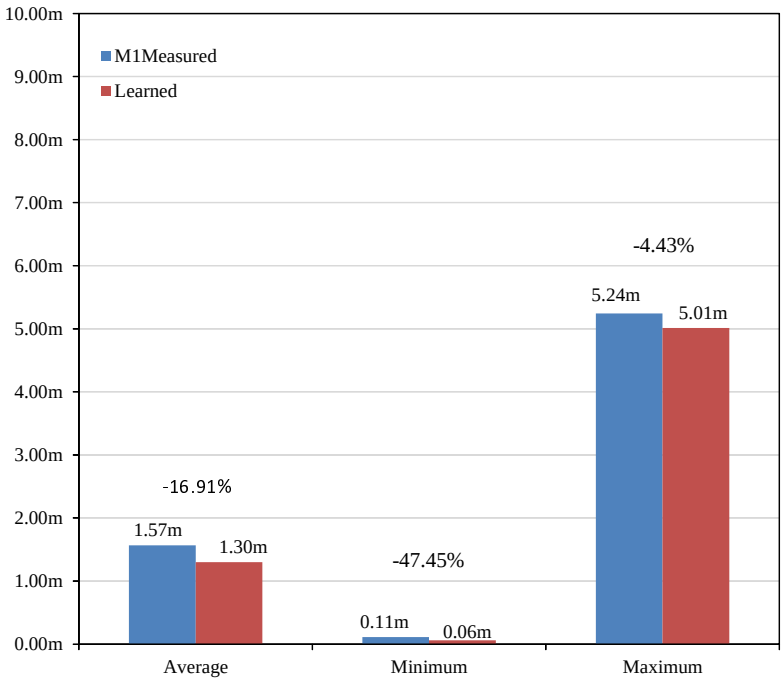

Figure 5.10: Average, Minimum and Maximum error between actual orbit and estimated position of vehicle

5.1.5 Correction Result

To confirm the usefulness of the proposed accuracy improvement system of the position identification of the vehicle, we conducted simulation experiments. Here, it is noted that the test data of the HNN in this section is different from the learning data.

First, Figure 5.11 shows measured data input to the HNN. Next, Figure 5.12 shows the simulation result of the proposed system expressed on X-Y coordinate. The plotted point in the figure means the estimated position of the vehicle by the HNN. From this figure, the HNN is tend to output the estimated position of the vehicle so that the output of the HNN agrees with the actual orbit.

As regards the error of the HNN output, it has periodically characteristics as shown in Figure 5.13. The X-axis indicates time [sec] and the Y-axis indicates the error between the actual orbit and the estimated position by the HNN. From this figure, we can see that the maximum error is approximately 8 meters although the minimum is less than 1 meter. Figure 5.14 shows the average, minimum and maximum error between the actual orbit and the estimated position of the vehicle. Average error, minimum error, and maximum error are improved approximately 18.62%, 6.17%, 10.5%, respectively.

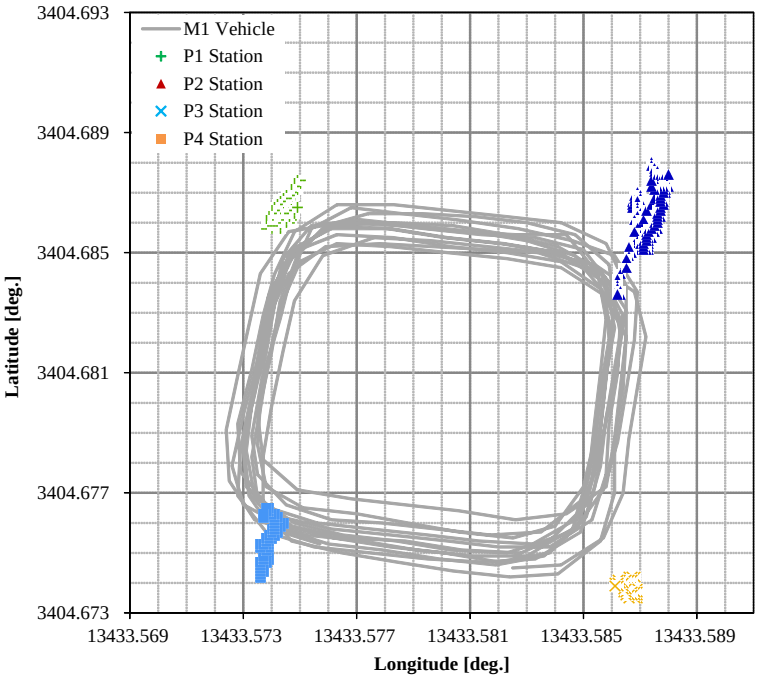

Figure 5.11: Measurement results of each GNSS unit [for simulation]

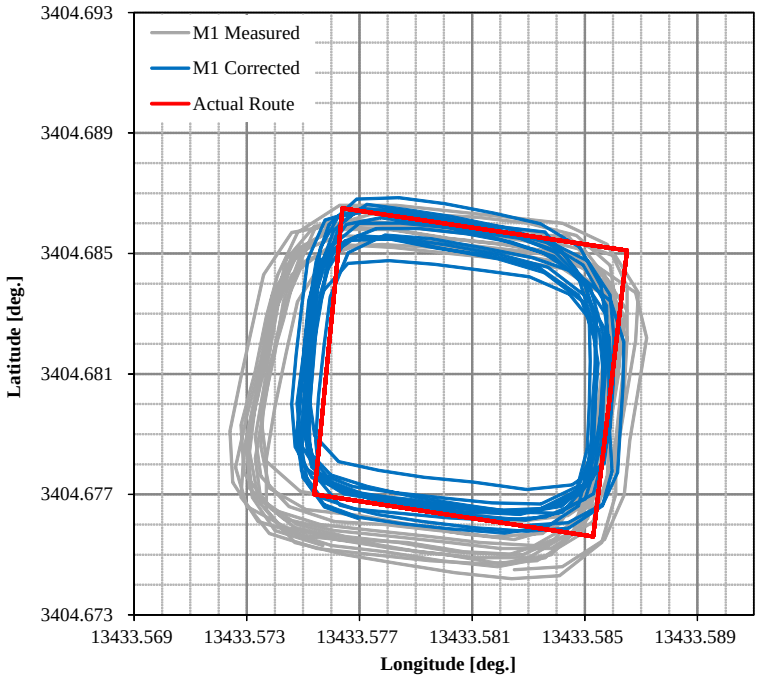

Figure 5.12: Simulation result of HNN expressed on X-Y coordinate

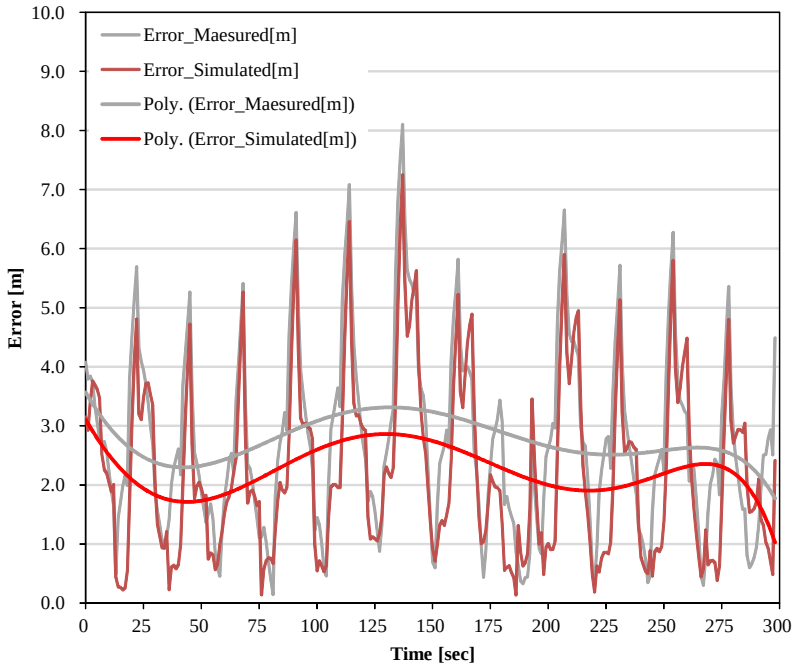

Figure 5.13: Simulation result of the error between the actual orbit and the simulation output position by the HNN

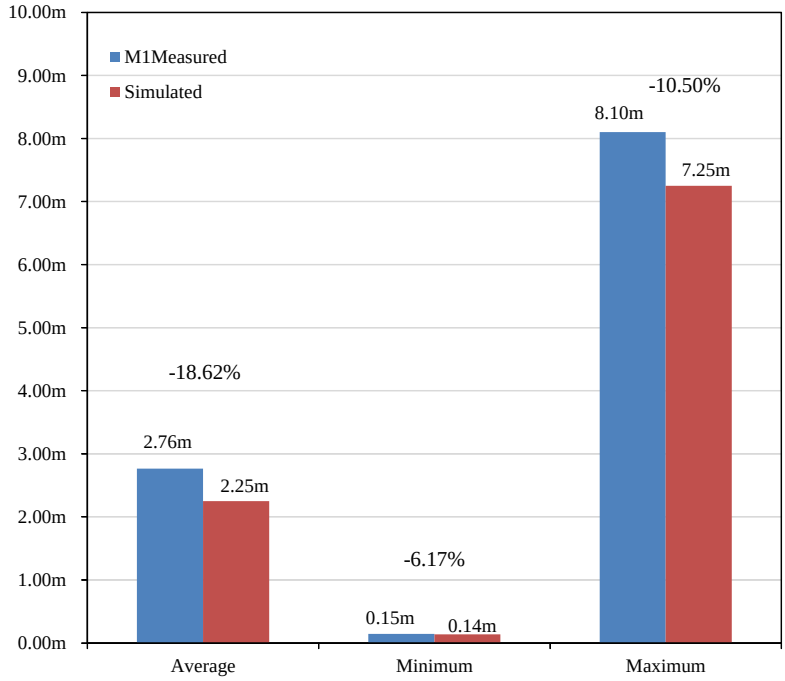

Figure 5.14: Simulation result of the error between the actual orbit and the estimated position by the HNN

5.2 Position Correction by Satellite Ephemeris

It is possible to express in 2 dimensional vector from the relative positions of each satellite and the receiver. Positioning errors are predictable and correctable from the inner product of these vectors. Equation (5.5) and Equation (5.6) show the correction equations for the latitude and the longitude.

$$Lat' = Lat + \sum(\cos(h) * \cos(450 - A)) * k \tag{5.5}$$

$$Lon' = Lon + \sum(\cos(h) * \sin(450 - A)) * k \tag{5.6}$$

where h and A mean the current satellite elevation and azimuth from a surface of the receiver. k means a correcting coefficient from the characteristic of the receiver.

5.2.1 Position Measurement

I measured GNSS position during 24 hours at fixed position to determine the correcting coefficient k and make a database for the correction. Locosys LS200301 GNSS module is used for the measurement. The positioning rate is 10 Hz. The environment was clear weather with no any interferences or obstacles.

5.2.2 Measurement Result

Figure 5.15 and Figure 5.16 show results of the measured positions and analysis. Position errors are occurred for all direction randomly from the actual position. Maximum error is approximately 7 m, while average error is approximately 2 m.

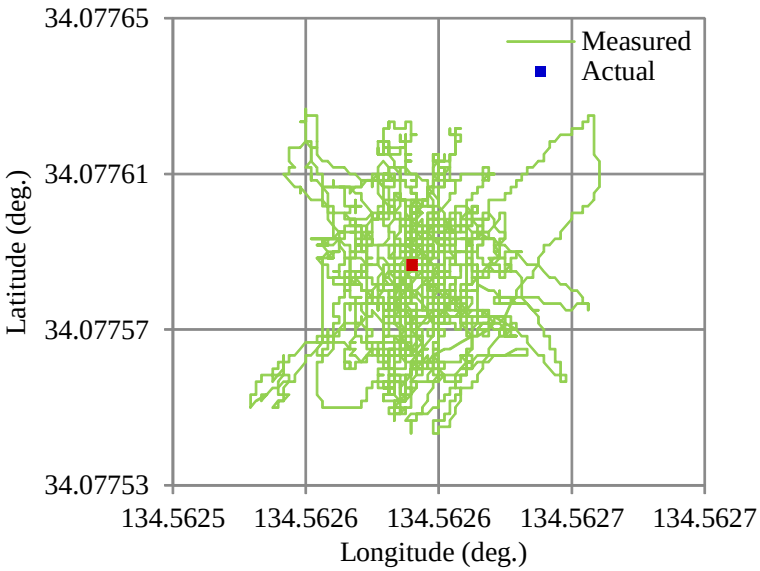

Figure 5.15: Measured positions

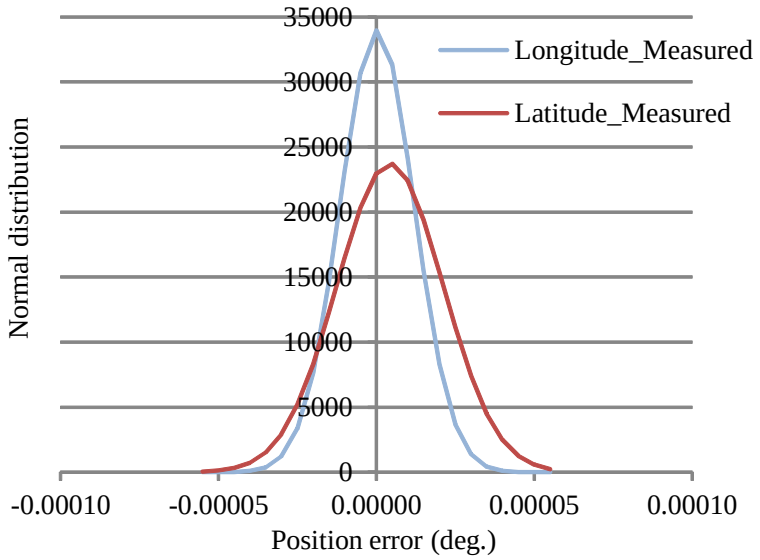

Figure 5.16: Error distribution

5.2.3 Correction Result

Figure 5.17 and Figure 5.18 show analysis of correction results. The most frequently occurred distance error is decreased to approximately 1.8 m from approximately 2 m. Furthermore, latitude error is concentrated to zero before than correction. However, over 6 m distance errors still exist.

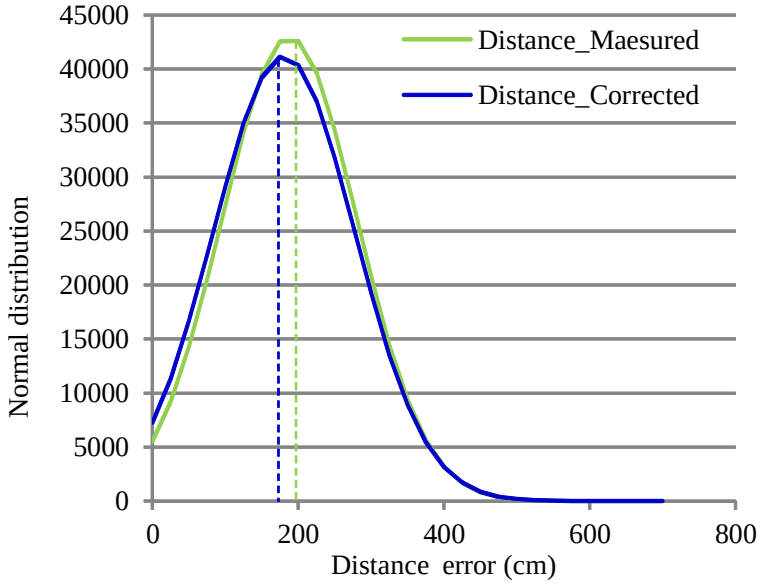

Figure 5.17: Results analysis of correction distances

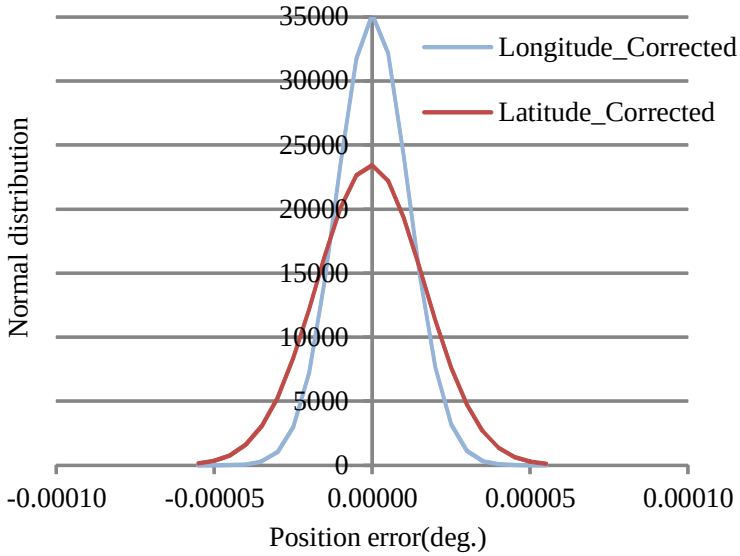

Figure 5.18: Results analysis of error distribution

5.3 Position Correction by Vehicle Dynamics

In order to improve positioning reliability and stability, each of the position is corrected by the proposed position correction algorithm which is based on vehicle dynamics [68]. Current velocity and heading angle are measured by velocity and heading angle feedback of the system. Thus, next coordinate prediction is possible by measured absolute values and current coordinate. When vehicle driving, the system compares the GNSS value and system feedback value. Therefore, the impossible movement is corrected by the algorithm. When vehicle stopping, the correction algorithm averages coordinates, and current coordinate is changed to the averaged coordinate that in order to stabilize positioning. The correction algorithm is simulated that in order to evaluate usability [69]-[71].

5.3.1 Correction Algorithm in Driving

When the vehicle driving, the system calculates current velocity and heading angle from the system status feedback. Simultaneously, current velocity and heading angle are calculated by trajectory which is recorded by the GNSS. Subsequently, the system compares the calculated values by the GNSS with the system feedback. If the difference of heading angle is over 17.5 degrees, coordinate is corrected by correction equation (5.7).

$$\begin{bmatrix} x' \\ y' \end{bmatrix} = \begin{bmatrix} x_p \\ y_p \end{bmatrix} + k \begin{bmatrix} \cos\theta & -\sin\theta \\ \sin\theta & \cos\theta \end{bmatrix} \begin{bmatrix} x_{c-p} \\ y_{c-p} \end{bmatrix} \tag{5.7}$$

where x and y are the longitude and the latitude. x' and y' are the corrected coordinate which can be calculated by the coordinate rotation equation in triangular function. x_p and y_p are the latest coordinate which excepts current measured coordinate by the GNSS. x_{c-p} and y_{c-p} are the longitude and latitude variations between current and past coordination by the GNSS without correction. θ denotes the difference angle. k denotes the velocity rate which is divided value of absolute velocity with calculated velocity by the GNSS. The reference angle is determined by the turning characteristic of vehicle dynamics. In addition, distance of the trajectory is corrected by velocity comparison.

5.3.2 Correction Algorithm in Stopping

When the vehicle in stopping, absolute coordinate never be changed. Thus, the system averages 100 coordinates for position stabilization during 20 seconds with 0.2 second sampling rate. The reason why, conventional waiting time for traffic signal is least 20 seconds in normal traffic [72], [73]. Furthermore, the coordinate is changed maximum 10 cm in one sampling of the GNSS receiver module which is implemented in the system. In that case, if averaging over 100 samples, coordinate is changed less than 1 mm at the last averaging. Therefore, the correction algorithm averages latest 100 coordinates, and current coordinate is changed to the averaged coordinate. If the vehicle stopped for 20 seconds, the algorithm averages every coordinate until the vehicle starts to moving.

5.3.3 Correction Result for Driving

The simulation results of correction algorithm for driving are listed in Table 5.2. Least 24.24% of coordinates are corrected by the algorithm. Correction distances are distributed 0.17 cm to 42.68 cm, and average correction distance is 14.13 cm in the one sampling.

Table 5.2: Correction rate and performance

	A	B	Average
Number of total coordinate	883	883	883
Number of corrected coordinate	214	261	237.5
Correction rate	24.24%	29.56%	26.90%
Minimum correction distance	0.17 cm	0.28 cm	0.23 cm
Maximum correction distance	40.64 cm	42.68 cm	41.66 cm
Average correction distance	14.59 cm	13.67 cm	14.13 cm

Figure 5.19 shows the correction simulation result of vehicle A as the preceding vehicle. In the result, when the vehicle drives in curve course, the more coordinates are corrected than straight line course.

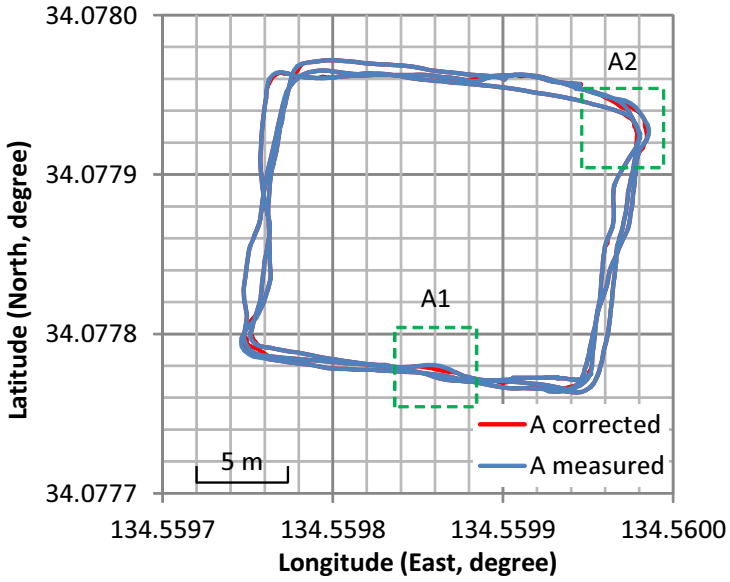

Figure 5.19: Correction result of the vehicle A in driving

Figure 5.20 and Figure 5.21 are shown in detailed view at Point A1 and Point A2 in Figure 5.19. The side draft is corrected by the algorithm in the straight line course at the Point A1. The overshoot is corrected by the algorithm in the curve course at Point A2.

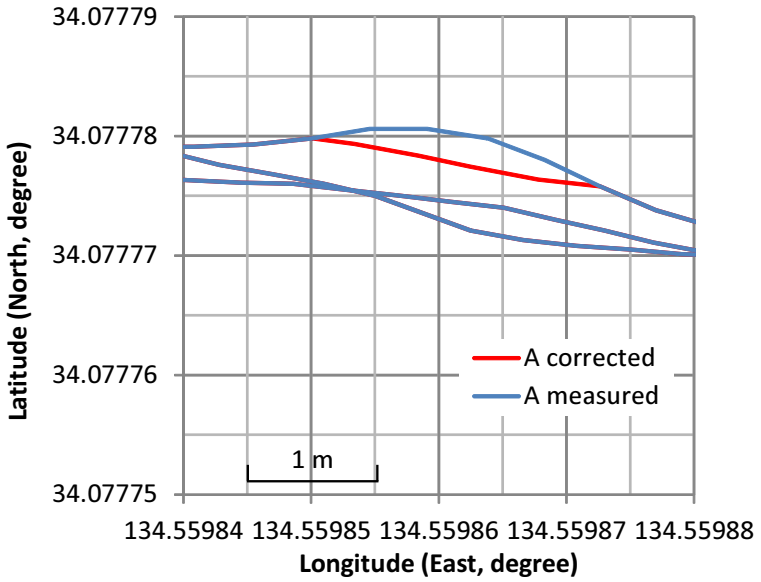

Figure 5.20: Coordinate correction of vehicle A in the straight line course A1

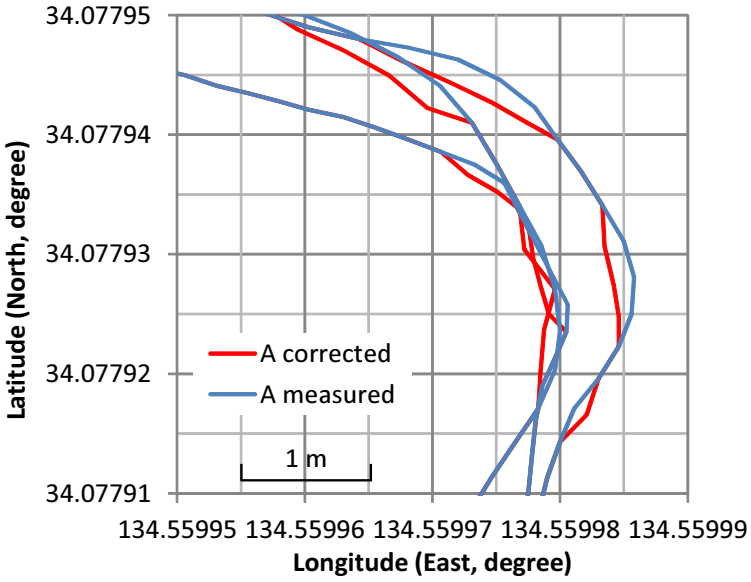

Figure 5.21: Coordinate correction of vehicle A in the curve course A2

Figure 5.22 shows the correction simulation result of vehicle B as the following vehicle. Likewise with vehicle A, when the vehicle drives in curve course, the more coordinates are corrected than straight line course.

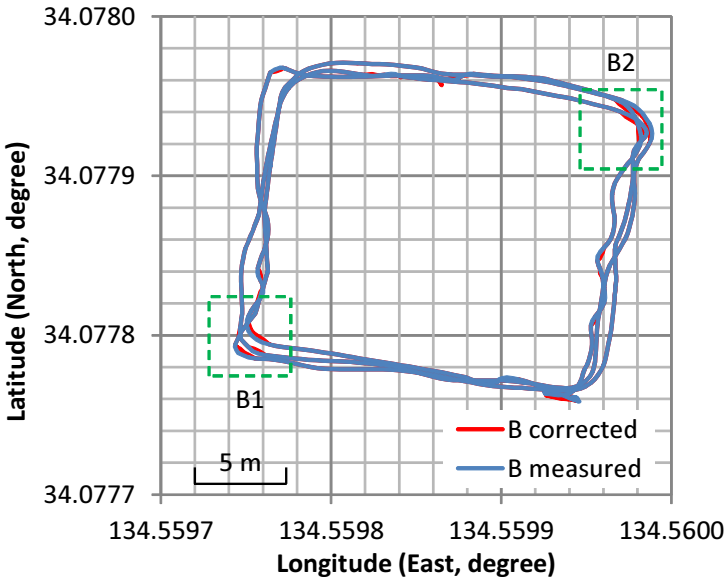

Figure 5.22: Correction result of the vehicle B in driving

Figures 5.23 and 5.24 are show detailed view of Point B1 and Point B2 in Figure 5.22. The overshoot is corrected by the algorithm in the curve course at the Point B1 and Point B2.

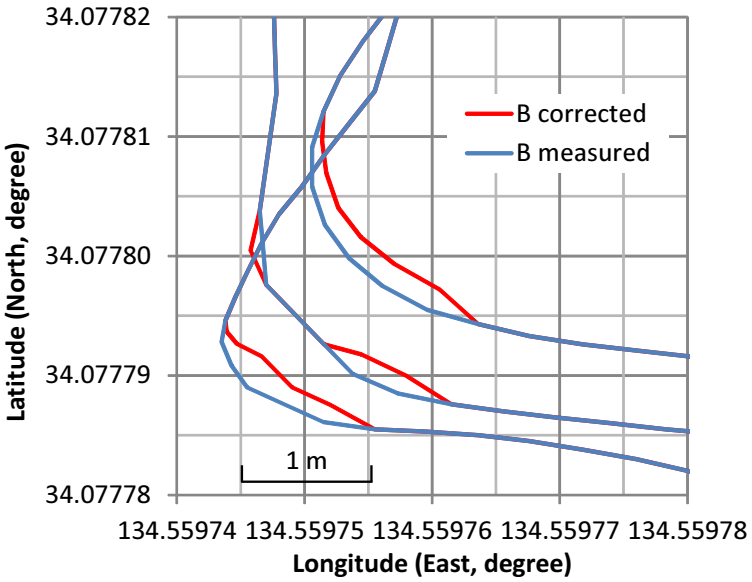

Figure 5.23: Coordinate correction of vehicle B in the curve course B1

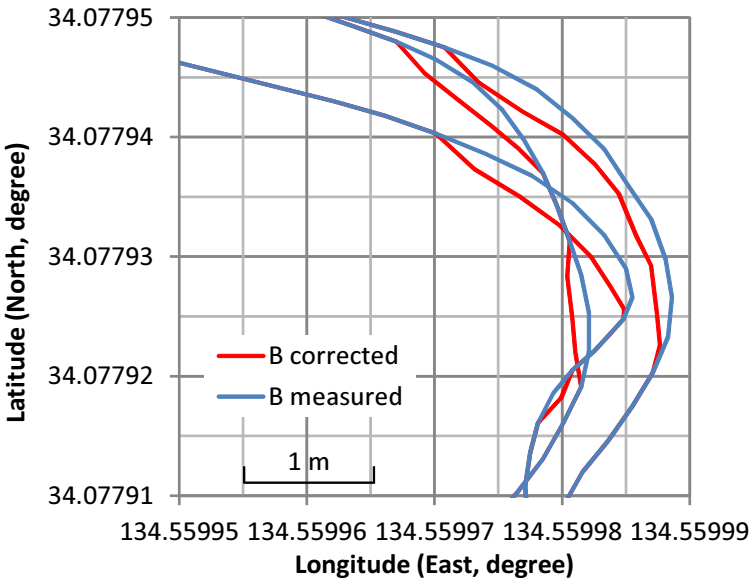

Figure 5.24: Coordinate correction of vehicle B in the curve course B2

5.3.4 Correction Result for Stop

The simulation result of correction algorithm in stopping is listed in Table 5.3. Mean, 1σ, 2σ values of the one dimension RMS errors are decreased to 45 cm (-15.09%), 84 cm (-14.29%), 116 cm (-16.55%) in relative mode by correction algorithm which averages latest 100 coordinate samples in stopping. However, the mean values of the single mode are slightly decreased or not decreased. From these result, improvement of position accuracy has confirmed by correction algorithm for stopping in the relative mode.

Table 5.3: RMS error (100 coordinates average)

Type	100 avg. Mean	100 avg. RMS 1σ	100 avg. RMS 2σ
Independent (A)	163 cm (0%)	215 cm (-4.02%)	267 cm (-4.3%)
Independent (B)	153 cm (-2.55%)	196 cm (-5.31%)	233 cm (-8.27%)
Relative (A,B)	45 cm (-15.09%)	84 cm (-14.29%)	116 cm (-16.55%)

Figure 5.25 shows normal distributions comparison of normal positioning and positioning with correction algorithm in stopping. The distribution curve of corrected positioning shows more narrow distribution band than normal positioning. It means that the positioning precision is improved by the correction method.

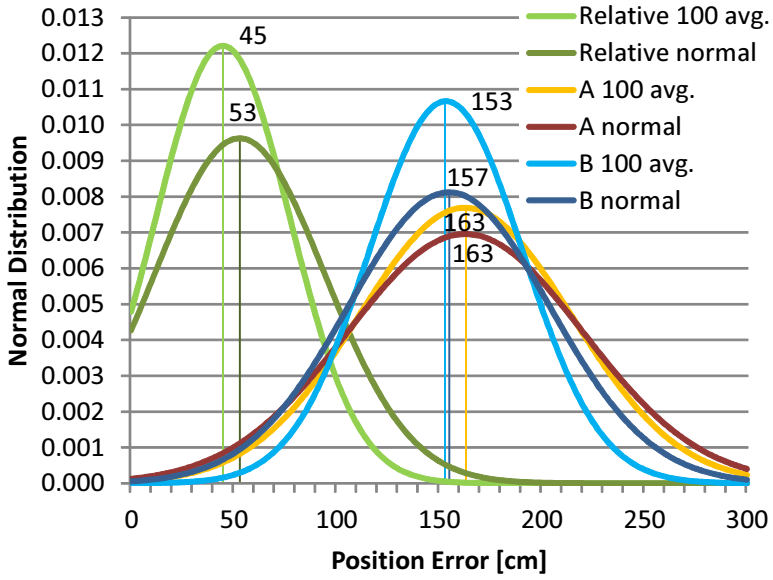

Figure 5.25: Distributions of RMS error by correction algorithm in stopping

5.4 Position Correction by Multiple GNSS

In order to improve positioning reliability and stability, each of the position is corrected by the proposed correction algorithm which is based on multiple GNSS modules. Generally, a received coordinate of GNSS module has uncertainty. When two GNSS modules are installed at the same position, selected satellite set for GNSS positioning are different from each other. In addition, uncertainty and coordinate are also different. The uncertainty is random component. Therefore, if a coordinate is calculated by multi GNSS receivers, the uncertainty would be decrease with high probability. When two GNSS receiver modules are on the ideal receiving situation, an average coordinate of two modules is the true center position of two modules. However, receiving environment is not ideal situation. In addition, positioning reliability is also different from each other. Therefore, this study proposes a weighted averaging method which using the ratio of HDOPs from two modules. Equation (5.8) and Equation (5.9) show the proposed method.

$$\begin{bmatrix} x' \\ y' \end{bmatrix} = \begin{bmatrix} x_1 \\ y_1 \end{bmatrix} + k \begin{bmatrix} x_2 - x_1 \\ y_2 - y_1 \end{bmatrix} \tag{5.8}$$

$$k = \frac{HDOP_1}{HDOP_1 + HDOP_2} \tag{5.9}$$

where x' and y' are corrected longitude and latitude. x_n and y_n are current coordinates which measured by each GNSS module. $HDOP_1$ and $HDOP_2$ are current values of the horizontal dilution of precision which are indicated by each GNSS module.

5.4.1 Measurement Condition

In order to evaluate weighted averaging correction method, GNSS coordinate and receiving status had logged during approximately 3 hours from two GNSS modules at a fixed position. Distance between modules is approximately 130 mm. Weather was clear. There was no any GNSS receiving interference obstacle during the measurement.

5.4.2 Measurement Result

Figure 5.26 shows measured coordinates from each GNSS module. Distribution of position error is similar each other. Remarkable irregular position error is occurred from two modules. Sudden position error would be a reason for unstable self-driving.

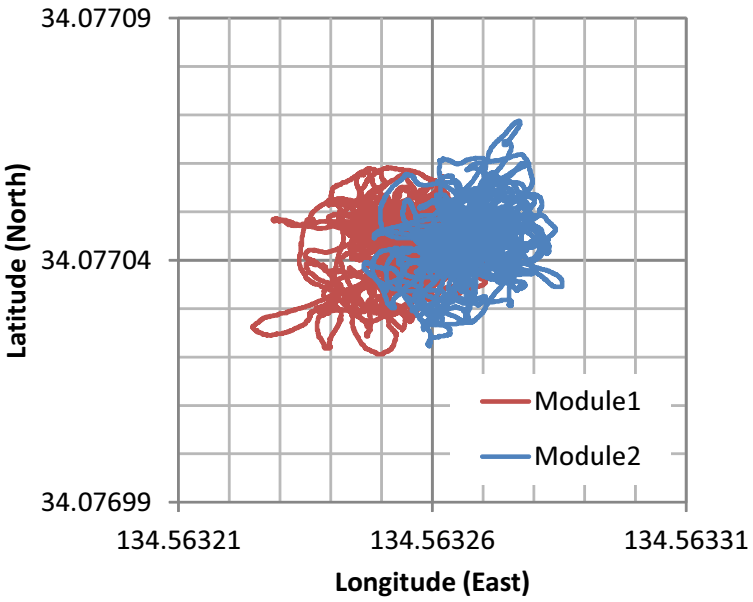

Figure 5.26: Measurement result from dual GNSS module

5.4.3 Correction Result

Weighted averaging correction result is shown in Table 5.4 and Figure 5.27. Almost average coordinate is located between two modules. In addition, sudden irregular error is suppressed by correction algorithm remarkably. Figure 5.28 indicates normal distribution of coordinates. Standard deviation is decreased approximately -52.16 %. Mean position error is decreased approximately -25.94 %. In other words, concentration level and stability is increased by correction algorithm.

Table 5.4: Correction rate and performance

	Module1	Module2	Corrected
Number of total coordinate	116916	116916	116916
Time span of total coordinate	3 hour	3 hour	3 hour
Mean Position Error	88.87 cm	86.62 cm	64.98 cm (-25.94%)
Minimum Position Error	1.25 cm	1.76 cm	0.98 cm (-34.88%)
Maximum Position Error	312.49 cm	298.81 cm	210.53 cm (-31.12%)
Standard Deviation	88.87	86.62	35.59 (-52.16)

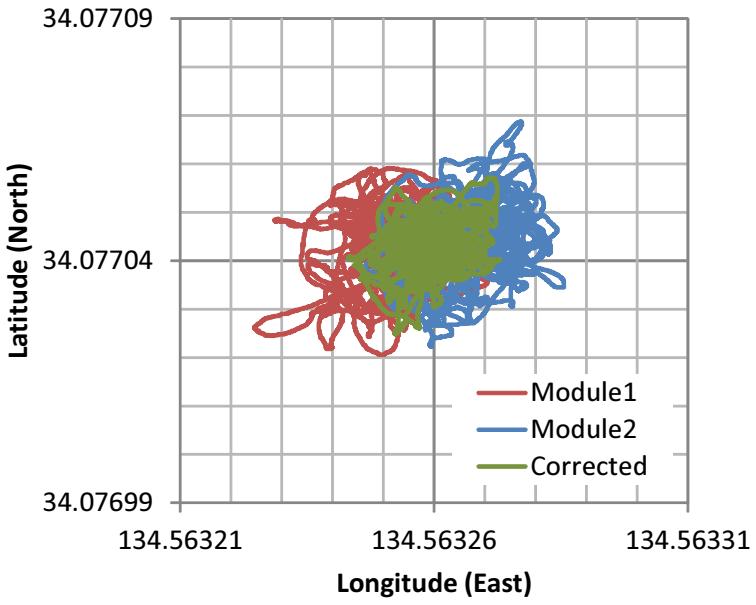

Figure 5.27: Averaging result by dual GNSS module

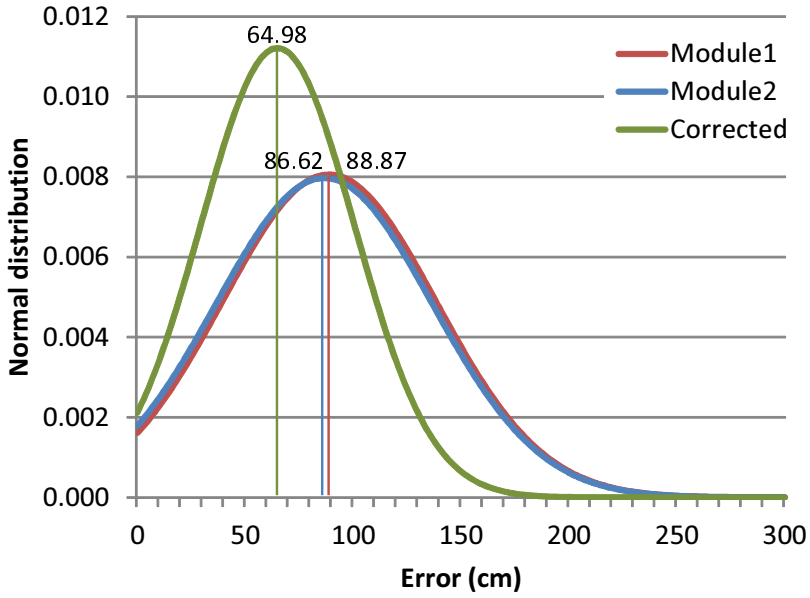

Figure 5.28: Normal distribution of position errors

Chapter 6

Conclusion

In this study, two type of self-driving systems are proposed. First one is a single mode self-driving system with GNSS positioning. The other is a platooning mode self-driving system with GNSS using a relative distance between preceding and following vehicles. Both type of self-driving systems have obstacle collision prevention stop algorithms. In addition, several correction method has applied to system. To ensure the validity of the proposed system, several experiments and simulations were conducted. As a result, the proposed single mode self-driving system implemented in the compact vehicle performed successfully for approaching to several fixed way points and destination point. The proposed platooning self-driving system implemented in the follower vehicle performed successfully for tracking to moving preceding vehicle. Furthermore, according to the results of simulations, the positioning accuracy and precision has improved by correction algorithms which are based on the neural network, satellite ephemeris, vehicle dynamics and weighted averaging by multiple GNSS module. Although the remaining absolute position error of the GNSS data, the measurement accuracy of multiple GNSS weighted averaging and the relative distance between the vehicles were improved.

In the future, In order to improve the performance of position reliability with minimum error, we plan to complex correction method by more than two methods to realize a complete self-driving system with single mode self-driving vehicle.

Appendix A

Appendix

A.1 CAN Message List and Description

ID	Group (Module)	Title	Description (&Enable/Disable, Span)
000	External Emergency	External Emergency Stop	Stop for All of the Functions Immediately
020	Internal Emergency	Internal Emergency Stop	Stop for All of the Functions Immediately
021	Internal Emergency	Low Voltage Warning (12VDC)	Low Voltage Warning (12VDC)
022	Internal Emergency	Low Voltage Warning (48VDC)	Low Voltage Warning (48VDC)
023	Internal Emergency	Obstacle Stop by Front Ultrasonic	Obstacle Stop by Front Ultrasonic (0 normal, 1 stop)
080	Exernal Command	Device Access Request	Device Access Request
081	Exernal Command	Digital Compass Calibration	Digital Compass Calibration
0A0	Internal Command	Drive Mode	N/A for High Priority Message
0A1	Internal Command	Self-Driving Start	N/A for High Priority Message
0A2	Internal Command	Self-Driving Pause / Resume	N/A for High Priority Message
0A3	Internal Command	Self-Driving Terminate	N/A for High Priority Message
180	Navigator	Remain Distance	N/A for High Priority Message
181	Navigator	Target angle (Global)	N/A for High Priority Message
182	Navigator	Waypoint Number	N/A for High Priority Message
200	Switch	Drive Mode Selector	-
201	Switch	Break Mode Selector	-
202	Switch	Steering Mode Selector	-

Figure A.1: CAN ID List and description 1/5

203	Switch	Throttle Mode Selector	-
204	Switch	Go & Stop	Auto Pilot Start or Terminate
205	Switch	DRL	-
206	Switch	Hazard Switch	-
207	Switch	Turn Signal LH	-
208	Switch	Turn Signal RH	-
209	Switch	Seatbelt LH	-
20A	Switch	Seatbelt RH	-
250	Brake	Brake Mode	Autonomous or Manual or Double
251	Brake	Target Brake Command	Disc & Regeneration Brake Pushing Forces
252	Brake	Brake On	Broadcasts Brake On status to the Bus
253	Brake	Brake Position Sensor	Disc Brake Wire Position
254	Brake	Brake Pedal Sensor	Brake Pedal Position
255	Brake	Regeneration Deceleration	Rate of Regeneration Deceleration
260	Steering	Steering Mode	Autonomous or Manual
261	Steering	Target Steering Angle	-
262	Steering	Steering Smoothness Factor	-
263	Steering	Current Steering Position	-
270	Throttle	Thrrotle Mode	Autonomous or Manual
271	Throttle	Target Throttle Command	-
272	Throttle	Thrrotle Direction Commnad	-
273	Throttle	Throttle On	-
274	Throttle	Current Vehicle Velocity	Current Velocity of Vehicle (Average)
275	Throttle	Velocity LH	Current Velocity of Left Wheel
276	Throttle	Velocity RH	Current Velocity of Right Wheel
277	Throttle	Throttle Pedal Sensor	Throttle Pedal Position
278	Throttle	Acceleration Average	-
279	Throttle	Acceleration LH	-
27A	Throttle	Acceleration RH	-
280	GNSS	Multi GNSS Mode	Indicator of the GNSS (1 Single L. 2 Single R, 3 Dual)
281	GNSS	Time (Average)	Current time by GNSS satellite atomic clock
282	GNSS	NS (Average)	Drafting direction for north or south
283	GNSS	Latitude High (Average)	Latitude high bit

Figure A.2: CAN ID List and description 2/5

284	GNSS	Latitude Low (Average)	Latitude low bit
285	GNSS	WE (Average)	Drafting direction for east or west
286	GNSS	Longitude High (Average)	Longitude high bit
287	GNSS	Longitude Low (Average)	Longitude low bit
28B	GNSS	NS (LH)	Drafting direction for north or south
28C	GNSS	Latitude High (LH)	Latitude high bit
288	GNSS	HDOP (Average)	HDOP indicator
289	GNSS	Receiving Balance Feedback	Calculated receiving balance from 2 modules
28A	GNSS	Single L GNSS Mode	GNSS Receiving Mode
28D	GNSS	Latitude Low (LH)	Latitude low bit
28E	GNSS	WE (LH)	Drafting direction for east or west
28F	GNSS	Longitude High (LH)	Longitude high bit
290	GNSS	Longitude Low (LH)	Longitude low bit
291	GNSS	HDOP (LH)	HDOP indicator
292	GNSS	SV Num (LH)	Number of SV
293	GNSS	Single R GNSS Mode	GNSS Receiving Mode
294	GNSS	NS (RH)	Drafting direction for north or south
295	GNSS	Latitude High (RH)	Latitude high bit
296	GNSS	Latitude Low (RH)	Latitude low bit
297	GNSS	WE (RH)	Drafting direction for east or west
298	GNSS	Longitude High (RH)	Longitude high bit
299	GNSS	Longitude Low (RH)	Longitude low bit
29A	GNSS	HDOP (RH)	HDOP indicator
29B	GNSS	SV Num (RH)	Number of SV
29C	GNSS	Velocity by GNSS Average	-
29D	GNSS	Velocity by GNSS LH	-
29E	GNSS	Velocity by GNSS RH	-
29F	GNSS	Balance Factor Fix (50%)	-
2C0	Ultrasonic	Ultrasonic Front 0 (LH)	SRF02 (I2C address: 0xE2)
2C1	Ultrasonic	Ultrasonic Front 1	SRF02 (I2C address: 0xE4)
2C2	Ultrasonic	Ultrasonic Front 2	SRF02 (I2C address: 0xE6)
2C3	Ultrasonic	Ultrasonic Front 3 (C)	SRF02 (I2C address: 0xE8)
2C4	Ultrasonic	Ultrasonic Front 4	SRF02 (I2C address: 0xEA)

Figure A.3: CAN ID List and description 3/5

2C5	Ultrasonic	Ultrasonic Front 5	SRF02 (I2C address: 0xEC)
2C6	Ultrasonic	Ultrasonic Front 6 (RH)	SRF02 (I2C address: 0xEE)
2C7	Ultrasonic	Ultrasonic Rear 0 (LH)	SRF02 (I2C address: 0xF0)
2C8	Ultrasonic	Ultrasonic Rear 1 (C)	SRF02 (I2C address: 0xF2)
2C9	Ultrasonic	Ultrasonic Rear 2 (RH)	SRF02 (I2C address: 0xF4)
2CA	Ultrasonic	Ultrasonic Judgement	Ultrasonic Judgement
2E0	Compass	Compass 0	HMC6352 (I2C address: 0xC0)
2E1	Compass	Compass 1	HMC6352 (I2C address: 0xC2)
2F0	Accelerometer	Accelerometer X	MPU-9250 (I2C address: 0xD2)
2F1	Accelerometer	Accelerometer Y	MPU-9250 (I2C address: 0xD2)
2F2	Accelerometer	Accelerometer Z	MPU-9250 (I2C address: 0xD2)
300	Gyroscope	Gyroscope X	MPU-9250 (I2C address: 0xD2)
301	Gyroscope	Gyroscope X	MPU-9250 (I2C address: 0xD2)
302	Gyroscope	Gyroscope X	MPU-9250 (I2C address: 0xD2)
310	Lidar	Lidar Valid	Lidar Valid
311	Lidar	Total Obstacle Number	-
312	Lidar	Ostacle Index 1	-
313	Lidar	Ostacle Index 2	-
314	Lidar	Ostacle Index 3	-
315	Lidar	Ostacle Index 4	-
316	Lidar	Obstacle 1 Representative Degree	-
317	Lidar	Obstacle 2 Representative Degree	-
318	Lidar	Obstacle 3 Representative Degree	-
319	Lidar	Obstacle 4 Representative Degree	-
31A	Lidar	Obstacle 5 Representative Degree	-
31B	Lidar	Obstacle 6 Representative Degree	-
31C	Lidar	Obstacle 7 Representative Degree	-
31D	Lidar	Obstacle 8 Representative Degree	-
31E	Lidar	Obstacle 9 Representative Degree	-
31F	Lidar	Obstacle 10 Representative Degree	-
320	Lidar	Obstacle 11 Representative Degree	-
321	Lidar	Obstacle 12 Representative Degree	-
322	Lidar	Obstacle 13 Representative Degree	-

Figure A.4: CAN ID List and description 4/5

323	Lidar	Obstacle 14 Representative Degree	-
324	Lidar	Obstacle 15 Representative Degree	-
325	Lidar	Obstacle 16 Representative Degree	-
326	Lidar	Obstacle 17 Representative Degree	-
327	Lidar	Obstacle 18 Representative Degree	-
328	Lidar	Obstacle 19 Representative Degree	-
329	Lidar	Obstacle 20 Representative Degree	-
32A	Lidar	Obstacle 1 Representative Distance	-
32B	Lidar	Obstacle 2 Representative Distance	-
32C	Lidar	Obstacle 3 Representative Distance	-
32D	Lidar	Obstacle 4 Representative Distance	-
32E	Lidar	Obstacle 5 Representative Distance	-
32F	Lidar	Obstacle 6 Representative Distance	-
330	Lidar	Obstacle 7 Representative Distance	-
331	Lidar	Obstacle 8 Representative Distance	-
332	Lidar	Obstacle 9 Representative Distance	-
333	Lidar	Obstacle 10 Representative Distance	-
334	Lidar	Obstacle 11 Representative Distance	-
335	Lidar	Obstacle 12 Representative Distance	-
336	Lidar	Obstacle 13 Representative Distance	-
337	Lidar	Obstacle 14 Representative Distance	-
338	Lidar	Obstacle 15 Representative Distance	-
339	Lidar	Obstacle 16 Representative Distance	-
33A	Lidar	Obstacle 17 Representative Distance	-
33B	Lidar	Obstacle 18 Representative Distance	-
33C	Lidar	Obstacle 19 Representative Distance	-
33D	Lidar	Obstacle 20 Representative Distance	-
33E	Lidar	H/W Fault	-
33F	Lidar	SW Fault	-
700	Information	Circuit Power Voltage Status (12VDC)	-
701	Information	Motor Power Voltage Status (48VDC)	-
702	Information	Estimated Driving Available Time	-
7FF	Information	Default Message	Default CAN ID for TXRX Test (No function)

Figure A.5: CAN ID List and description 5/5

A.2 Front Wheel Differential Characteristic

Steering angle	Diff. Rate	Speed (Km/h) ※Inside Wheel Slow(−), Outside Wheel Fast(+)						
		5	10	15	20	25	30	40
0	100.00%	5.00	10.00	15.00	20.00	25.00	30.00	40.00
1	100.30%	5.02	10.03	15.05	20.06	25.08	30.09	40.12
2	100.60%	5.03	10.06	15.09	20.12	25.15	30.18	40.24
3	100.90%	5.05	10.09	15.14	20.18	25.23	30.27	40.36
4	101.20%	5.06	10.12	15.18	20.24	25.30	30.36	40.48
5	101.50%	5.08	10.15	15.23	20.30	25.38	30.45	40.60
6	101.80%	5.09	10.18	15.27	20.36	25.45	30.54	40.72
7	102.10%	5.11	10.21	15.32	20.42	25.53	30.63	40.84
8	102.40%	5.12	10.24	15.36	20.48	25.60	30.72	40.96
9	102.70%	5.14	10.27	15.41	20.54	25.68	30.81	41.08
10	103.00%	5.15	10.30	15.45	20.60	25.75	30.90	41.20
11	103.30%	5.17	10.33	15.50	20.66	25.83	30.99	41.32
12	103.60%	5.18	10.36	15.54	20.72	25.90	31.08	41.44
13	103.90%	5.20	10.39	15.59	20.78	25.98	31.17	41.56
14	104.20%	5.21	10.42	15.63	20.84	26.05	31.26	41.68
15	104.50%	5.23	10.45	15.68	20.90	26.13	31.35	41.80
16	104.80%	5.24	10.48	15.72	20.96	26.20	31.44	41.92
17	105.10%	5.26	10.51	15.77	21.02	26.28	31.53	42.04
18	105.40%	5.27	10.54	15.81	21.08	26.35	31.62	42.16
19	105.70%	5.29	10.57	15.86	21.14	26.43	31.71	42.28
20	106.00%	5.30	10.60	15.90	21.20	26.50	31.80	42.40
21	106.30%	5.32	10.63	15.95	21.26	26.58	31.89	42.52
22	106.60%	5.33	10.66	15.99	21.32	26.65	31.98	42.64
23	106.90%	5.35	10.69	16.04	21.38	26.73	32.07	42.76
24	107.20%	5.36	10.72	16.08	21.44	26.80	32.16	42.88
25	107.50%	5.38	10.75	16.13	21.50	26.88	32.25	43.00
26	107.80%	5.39	10.78	16.17	21.56	26.95	32.34	43.12
27	108.10%	5.41	10.81	16.22	21.62	27.03	32.43	43.24
28	108.40%	5.42	10.84	16.26	21.68	27.10	32.52	43.36
29	108.70%	5.44	10.87	16.31	21.74	27.18	32.61	43.48
30	109.00%	5.45	10.90	16.35	21.80	27.25	32.70	43.60

Figure A.6: Characteristic of Software Differential for Front Wheels

◇ ◇ ◇ ◇ References ◇ ◇ ◇ ◇

[1] Gregory Kehoe, Hossein Jula, Fariba Ariaei, "Developing Successful Autonomous Ground Vehicles: Lessons Learned from DARPA Challenges", *12th IFAC Symposium on Transportation Systems, Year Organization*, pp. 399-406, 2009. 8

[2] Byung-Hyun Lee, Jong-Hwa Song, Jun-Hyuck Im, Sung-Hyuck Im, Moon-Beom Heo, Gyu-In Jee, "GPS/DR Error Estimation for Autonomous Vehicle Localization", *Sensors 2015,15, 20779-20798*, pp. 20779-20798, 2015.

[3] H. Jung, "An efficient lane detection algorithm for lane departure detection", *Intelligent Vehicles Symposium (IV), 2013 IEEE*, pp. 976-981, 2013. 06

[4] Johan Bengtsson, "Adaptive Cruise Control and Driver Modeling", *Lund Institute of Technology*, 2001.11

[5] K.A. Sidorenko, A.A. Vasenina, "Ionospheric parameters estimation using GLONASS/GPS data", *Advances in Space Research*, Volume 57, Issue 9, pp.1881-1888, 2016.5.1

[6] Martin Lad, Ivo Herman, Zden?k Hurak, "Vehicular platooning experiments using autonomous slot cars", *IFAC-PapersOnLine*, Volume 50, Issue 1, pp.12596-12603, 2017.7

[7] Eric R. Teoh, David G. Kidd, "Rage against the machine? Google's self-driving cars versus human drivers", *Journal of Safety Research*, Volume 63, pp.57-60, 2017.12

[8] M. Konig, L. Neumayr, "Users' resistance towards radical innovations: The case of the self-driving car", *Transportation Research Part F: Traffic Psychology and Behaviour*, Volume 44, pp.42-52, 2017.1

[9] Cyriel Diels, Jelte E. Bos, "Self-driving carsickness", *Applied Ergonomics*, Volume 53, Part B, pp.374-382, 2016.3

[10] Nynke E. Vellinga, "From the testing to the deployment of self-driving cars: Legal challenges to policymakers on the road ahead", *Computer Law & Security Review*, Volume 33, Issue 6, pp.847-863, 2017.12

[11] Qingsheng Kong, Shenglei Xu, Sang-sun Lee, "Using PDOP to Estimate Kalman Filter's Measurement Noise Covariance for GPS Positioning", *ICTTE 2012, IPCSIT vol. 26, IACSIT Press, Singapore*, pp. 33-37, 2012.

[12] Maryam Kamali, Louise A. Dennis, Owen McAree, Michael Fisher, Sandor M. Veres, "Formal verification of autonomous vehicle platooning", *Science of Computer Programming*, Volume148, pp.88-106, 2017.11.15

[13] Md Sharikur Rahman, Mohamed Abdel-Aty, "Longitudinal safety evaluation of connected vehicles' platooning on expressways", *Accident Analysis & Prevention*, In press, corrected proof, Available online 21 2017.12

[14] Baibing Li, "Stochastic modeling for vehicle platoons (II): Statistical characteristics", *Transportation Research Part B: Methodological*, Volume 95, pp.378-393, 2017.1

[15] S. Konduri, P.R. Pagilla, S. Darbha, "Vehicle Platooning with Multiple Vehicle Look-ahead Information", *IFAC-PapersOnLine*, Volume 50, Issue 1, pp.5768-5773, 2017.7

[16] Bradford W. Parkinson, Penina Axelrad, "Global Positioning System: Theory and Applications, Volume U", *American Institute of Aeronautics and Astronautics*, pp. 3-4, 1996.

[17] Marcus G. Ferguson, "Global Positioning System (GPS) error source prediction", *American Institute of Aeronautics and Astronautics*, pp. 8-10, 2000. 3

[18] Milad Azarbad, Hamed Azami, Saeid Sanei, Ataollah Ebrahimzadeh, "New Neural Network-based Approaches for GPS GDOP Classification based on Neuro-Fuzzy Inference System, Radial Basis Function, and Improved Bee Algorithm", *Applied Soft Computing*, Volume 25, pp.285-292, 2014.12

[19] Jong-Min Yeom, Kyung-Soo Han, "Improved estimation of surface solar insolation using a neural network and MTSAT-1R data", *Computers & Geosciences*, Volume 36, Issue 5, pp.590-597, 2010.5

[20] M. Saraf, K. Mohammadi, M.R. Mosavi, "Classifying the Geometric Dilution of Precision of GPS satellites utilizing Bayesian decision theory", *Computers & Electrical Engineering*, Volume 37, Issue 6, pp.1009-1018, 2011.11

[21] Yunlong Teng, Jinling Wang, Qi Huang, "Minimum of Geometric Dilution of Precision (GDOP) for five satellites with dual-GNSS constellations", *Advances in Space Research*, Volume 56, Issue 2, pp.229-236, 2015.7.15

[22] Yunlong Teng, Jinling Wang, Qi Huang, "Mathematical minimum of Geometric Dilution of Precision (GDOP) for dual-GNSS constellations", *Advances in Space Research*, Volume 57, Issue 1, pp.183-188, 2016.1.1

[23] Chih-Hung Wu, Ya-Wei Ho, Li-Wun Chen, You-Dong Huang, "Discovering approximate expressions of GPS geometric dilution of precision using genetic programming", *Advances in Engineering Software*, Volume 45, Issue 1, pp.332-340, 2012.3

[24] Yong Wang, Xiubin Zhao, Chunlei Pang, Bo Feng, Liang Zhang, Haibo Tong, "BDS and GPS stand-alone and integrated attitude dilution of precision definition and comparison", *Advances in Space Research*, In press, corrected proof, Available online 2017.12.2

[25] Peter Steigenberger, Manuela Seitz, Sarah Bockmann, Volker Tesmer, Urs Hugentobler, "Precision and accuracy of GPS-derived station displacements", *Physics and Chemistry of the Earth 53-54*, pp. 72-79, 2010. 8

[26] Bi Liu, Yunlong Teng, Qi Huang, "GDOP minimum in multi-GNSS positioning", *Advances in Space Research*, Volume 60, Issue 7, pp.1400-1403, 2017.10.1

[27] Shuqiang Xue, Yuanxi Yang, "Understanding GDOP minimization in GNSS positioning: Infinite solutions, finite solutions and no solution", *Advances in Space Research*, Volume 59, Issue 3, pp.775-785, 2017.2.1

[28] Ch. Raja Sekhar, V.B.S. Srilatha Indira Dutt, G. Sasibhushana Rao, "GDoP estimation using Simulated Annealing for GPS and IRNSS combined constellation", *Engineering Science and Technology*, an International Journal, Volume 19, Issue 4, pp.1881-1886, 2016.12

[29] Zhimin Liu, Yangyang Li, Jinyun Guo, Fei Li, "Influence of higher-order ionospheric delay correction on GPS precise orbit determination and precise positioning", *Geodesy and Geodynamics*, Volume 7, Issue 5, pp.369-376, 2016.9

[30] Reza Ghoddousi-Fard, Francois Lahaye, "Evaluation of single frequency GPS precise point positioning assisted with external ionosphere sources", *Advances in Space Research*, Volume 57, Issue 10, pp.2154-2166, 2016.5.15

[31] G. Sivavaraprasad, D. Venkata Ratnam, "Performance evaluation of ionospheric time delay forecasting models using GPS observations at a low-latitude station", *Advances in Space Research*, Volume 60, Issue 2, pp.475-490, 2017.7.15

[32] Xin Liu, Qinyun Zhang, M. Shah, Z. Hong, "Atmospheric-ionospheric disturbances following the April 2015 Calbuco volcano from GPS and OMI observations", *Advances in Space Research*, Volume 60, Issue 12, pp.2836-2846, 2017.12.15

[33] J. Federico Conte, Claudio Brunini, "Ingestion of FORMOSAT-3/COSMIC GPS data into La Plata Ionospheric Model: A preliminary assessment", *Advances in Space Research*, Volume 60, Issue 3, pp.677-691, 2017.8.1

[34] Aly M. El-nagger, "Enhancing the accuracy of GPS point positioning by converting the signal frequency data to dual frequency data", *Alexandria Engineering Journal*, Volume 50, Issue 3, pp. 237–243, 2011.08

[35] J. William, "Global positioning system standard positioning service performance analysis report", *FAA GPS Performance Analysis Report*, 2014. 7

[36] Mohamad Hosein Refan, Adel Dameshghi, Mehrnoosh Kamarzarrin, "Improving RTDGPS accuracy using hybrid PSOSVM prediction model", *Aerospace Science and Technology 37*, pp. 55-69, 2014. 5

[37] T.H. Witte, A.M. Wilson, "Accuracy of WAAS-enabled GPS for the determination of position and speed over ground", *Journal of Biomechanics 38*, pp. 1717-1722, 2004. 7

[38] Lisa L. Arnold, Paul A. Zandbergen, "Positional accuracy of the Wide Area Augmentation System in consumer-grade GPS units", *Computers & Geosciences 37*, pp. 883-892, 2011. 3

[39] Atsushi Shimamura, "MSAS (MTSAT Satellite-based Augmentation System) Project Status", *Global Positioning System by ION, Volume VI*, 1999. 6

[40] Wang Bing, Sui Lifen, Xiao Gurui, Duan Yu, Qi Guobin, "Comparison of attitude determination approaches using multiple Global Positioning System (GPS) antennas", *Geodesy and Geodynamics*, Volume 4, Issue 1, pp. 16–22, 2013.02

[41] Maurice Schellekens, "Self-driving cars and the chilling effect of liability law", *Computer Law & Security Review*, Volume 31, Issue 4, pp.506-517, 2015.8

[42] Haifeng Zhang, Helen Beggs, Leon Majewski, Xiao Hua Wang, Andrew Kiss, "Investigating sea surface temperature diurnal variation over the Tropical Warm Pool using MTSAT-1R data", *Remote Sensing of Environment*, Volume 183, pp.1-12, 2016.9.15

[43] Toshihiro Hiraoka, Shota Takada "Collision Risk Evaluation Based on Deceleration for Collision Avoidance", *The Society of Instrument and Control Engineers* (SICE), Vol. 47, No.11, pp. 534-540, 2011

[44] Omae, M. "Development of Multi Purpose Small Electric Vehicle with Application of Automated Guiding Control System", *Journal of Asia Electric Vehicle* (JAEV), Vol. 2, No. 1 (2004), pp. 557-563

[45] John A. Klobuchar, "Ionospheric Effects on GPS", *Air Force Geophysics Laboratory, GPS world*, 1991. 4

[46] Paulo de Oliveria Camargo, Joao Francisco Galera Monico, Luiz Danilo Damasceno Ferreira, "Application of ionospheric corrections in the equatorial region for L1 GPS users", *Earth Planets Space, 52*, pp. 1083-1089, 2000.

[47] Johta Awano, Takahiko Ikeda, Michito Imae, "The Transistor Technology(In Japanese)", *CQ publishing company, ISSN 0040-9413*, pp. 41-88, 2016.02

[48] P Banerjee, Anindya Bose, "Evaluation of GPS PDOP from elevation and azimuth of satellites", *Indian Journal of Radio & Space Physics*, Vol. 25, April 1996, pp. 110-113, 1996

[49] Takimoto, Y., Raksincharoensak, P. and Nagai, M. , "Radar-Based Vehicle Following Control Algorithm of Micro-Scale Electric Vehicle", *Proceedings of 14th Asia Pacific Automotive Engineering Conference* (APAC), 2007-01-3590, pp. 1-6, 2017

[50] Christian Hane, Lionel Heng, Gim Hee Lee, Friedrich Fraundorfer, Paul Furgalef, Torsten Sattlerb, Marc Pollefeys, "3D visual perception for self-driving cars using

a multi-camera system: Calibration, mapping, localization, and obstacle detection", *Image and Vision Computing*, Volume 68, pp.14-27, 2017.12

[51] J. Navarro, M. Francois, F. Mars, "Obstacle avoidance under automated steering: Impact on driving and gaze behaviours", *Transportation Research Part F: Traffic Psychology and Behaviour*, Volume 43, pp.315-324, 2016.11

[52] Abdelkader Dairi, Fouzi Harrou, Mohamed Senouci, Ying Sun, "Unsupervised obstacle detection in driving environments using deep-learning-based stereovision", *Robotics and Autonomous Systems*, Volume 100, pp.287-301, 2018.2

[53] Pedram Gharani, Hassan A. Karimi, "Context-aware obstacle detection for navigation by visually impaired", *Image and Vision Computing*, Volume 64, pp.103-115, 2018.8

[54] Dong Han, Hong Nie, Jinbao Chen, Meng Chen, "Dynamic obstacle avoidance for manipulators using distance calculation and discrete detection", *Robotics and Computer-Integrated Manufacturing*, Volume 49, pp.98-104, 2018.2

[55] Hunjae Yoo, Jongin Son, Bumsub Ham, Kwanghoon Sohn, "Real-time rear obstacle detection using reliable disparity for driver assistance", *Expert Systems with Applications*, Volume 56, pp.186-196, 2016.9.1

[56] Jeffery Young, Milan Simic, "LIDAR and Monocular Based Overhanging Obstacle Detection", *Procedia Computer Science*, Volume 60, pp.1423-1432, 2015

[57] Ponlathep Lertworawanich, "Safe-Following Distances Based On The Car-Following Model", *PIARC International Seminar on Intelligent Transport System (ITS) In Road Network Operations*, 2006. 8

[58] Tiefang Zou, Zhi Yu, Ming Cai, Jike Liu, "Analysis and application of relationship between post-braking-distance and throw distance in vehicle?pedestrian accident reconstruction", *Forensic Science International 207*, pp. 135-144, 2010. 10

[59] Tom Urbanik, Alison Tanaka, Bailey Lozner, Eric Lindstrom, Kevin Lee, Shaun, Quayle, Scott Beaird, Shing Tsoi, Paul Ryus, Doug Gettman, Srinivasa Sunkari, Kevin Balke, Darcy Bullock, "Signal Timing Manual, Second Edition", *NCHRP Report 812, Transporation Research Board 2015*, 2015

[60] Kojima, Y., Suzuki, N., Hattori, Y. and Teramoto, E., "Precise Localization using Tightly Coupled Integration based on Trajectory estimated from GPS Doppler", *Proceedings of 10th AVEC Symposium* (2010), pp. 406-411

[61] Ali Tavasoli, Mahyar Naraghi, Heman Shakeri, "Optimized coordination of brakes and active steering for a 4WS passenger car", *ISA Transactions*, Volume 51, Issue 5, pp.573-583, 2012.9

[62] Milad Jalali, Saeid Khosravani, Amir Khajepour, Shih-ken Chen, Bakhtiar Litkouhi, "Model predictive control of vehicle stability using coordinated active steering and differential brakes", *Mechatronics*, Volume 48, pp.30-41, 2017.12

[63] Jingliang Duan, Renjie Li, Lian Hou, Wenjun Wang, Guofa Li, Bo Cheng, Shengbo Eben Li, Hongbo Gao, "Driver braking behavior analysis to improve autonomous emergency braking systems in typical Chinese vehicle-bicycle conflicts", *Accident Analysis & Prevention*, Volume 108, pp.74-82, 2017.11

[64] Wei-Tong Wang, Kuo-Feng Ssu, "Obstacle detection and estimation in wireless sensor networks", *Computer Networks*, Volume 57, Issue 4, pp.858-868, 2013.3.13

[65] Hanna Jeppsson, Martin Ostling, Nils Lubbe, "Real life safety benefits of increasing brake deceleration in car-to-pedestrian accidents: Simulation of Vacuum Emergency Braking", *Accident Analysis & Prevention*, Volume 111, pp.311-320, 2018.2

[66] Walter V. Wedig, "Velocity Jumps in Road-Vehicle Dynamics", *Procedia Engineering*, Volume 144, pp.1076-1085, 2016

[67] Bernhard Hofmann-Wellenhof, Herbert Lichtenegger, Elmar Wasle, "GNSS-Global Navigation Satellite Systems GPS, GLONASS, Galileo and more", *SpringerWienNewYork*, pp. 272-276, 2008.

[68] Chulliat, A., S. Macmillan, P. Alken, C. Beggan, M. Nair, B. Hamilton, A. Woods, V. Ridley, S. Maus, A. Thomson, "The US/UK World Magnetic Model for 2015-2020", *National Geophysical Data Center, NOAA* 2015.

[69] Shin Takehara, "The first step of vehicle dynamics (In Japanese)", *Morikita Publishing Co., Ltd.*, pp. 99-111, 2014. 10

[70] Junzhi Zhang, Yutong Li, Chen Lv, Jinfang Gou, Ye Yuan, "Time-varying delays compensation algorithm for powertrain active damping of an electrified vehicle

equipped with an axle motor during regenerative braking", *Mechanical Systems and Signal Processing*, Volume 87, Part B, pp.45-63, 2017.3.15

[71] Martina Jo?evski, Alexander Katriniok, Andreas Riek, Dirk Abel, "Disturbance Estimation for Longitudinal Vehicle Dynamics Control at Low Speeds", *IFAC-PapersOnLine*, Volume 50, Issue 1, pp.987-993, 2017.7

[72] Mustafa Elkady, Ahmed Elmarakbi, John MacIntyre, Mohammed Alhariri, "Collision mitigation and vehicle transportation safety using integrated vehicle dynamics control systems", *Journal of Traffic and Transportation Engineering (English Edition)*, Volume 4, Issue 1, pp.41-60, 2017.2

[73] S. Marisamynathan, P. Vedagiri, "Modeling Pedestrian Delay at Signalized Intersection Crosswalks under Mixed Traffic Condition", *Procedia - Social and Behavioral Sciences 104*, pp. 708-717, 2013. 11

Publications

【Main Paper】

1. “ Multiple Vehicles Semi-Self-driving System Using GNSS Coordinate Tracking under Relative Position with Correction Algorithm ” Heejin Lee, Hiroshi Suzuki, Takahiro Kitajima, Akinobu Kuwahara, Takashi Yasuno, International Journal of Advanced Computer Science and Applications, Vol.8, Page 418-426, September, 2017, Published

【Sub Paper】

1. “ Accuracy Improvement Method of Self-Localization for Outdoor Multiple Mobile Robots Using Neural Network” Heejin LEE, Takahiro KITAJIMA, Masaharu INOUE, Takashi YASUNO, Akinobu KUWAHARA, The Institute of Electronics, Information and Communication Engineers Technical Report, NC2015-12, Page 1-6, July, 2015, Published
2. “ Self-driving System Using GPS Coordinate Tracking under Relative Distance ” Heejin Lee, Hirosi Suzuki, Takashi Yasuno, Proceedings of the SICE Annual Conference 2016, The Society of Instrument and Control Engineers, Page 1050-1053, Tsukuba, JAPAN, September, 2016, Published

Acknowledgments

徳島大学の博士後期課程に入学し，本研究や論文が完成するまで，多方面でご指導をなさって下さった私の指導教授，安野 卓 先生に感謝の気持ちを申し上げます．そして，数年間アドバイスやサポートをなさって下さった理工学部の先生と職員の皆様にも感謝いたします．特に SKY Lab. の鈴木 先生，桑原 様，北島 様，高井 様，そして車輪チームの皆様には大変お世話になりました．心から感謝いたします．経済的に困難だった時，助けて下さった徳島大学の国際課の皆様，平和中島奨学財団の皆様にも感謝いたします．この徳島で無事に研究活動ができるようにまるで家族のように笑顔でサポートして下さった山西 様，矢野 様を始めて，留学期間中に出会って知り合いになった皆様にも感謝いたします．おかげさまで苦しい時も諦めたかった時も克服することができました．母国でいつも自分の研究を心配して下さっていた韓国海洋大学の教授の方々にも感謝いたします．博士後期課程に入学することを支援，応援して下さった家族の皆にも感謝します．特に，結婚の直後から大変なことばかりで苦しい生活を続けながらも今まで自分を支援してくれた妻に大変感謝しています．この研究が自分の成長のきっかけになり，この社会の中でますます活躍することができることを，それと共に自分の家族やお世話になった皆様に恩返しできることを心よりお祈り申し上げます．

末筆ながら，本日，この論文を 3 周年の結婚記念日を迎え，妻にプレゼントします．

2018 年 3 月 1 日